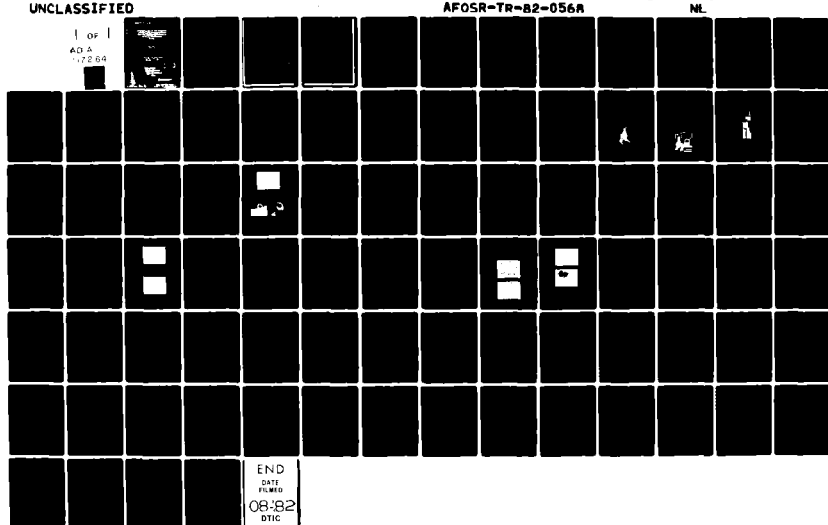


AD-A117 264

SPECTRON DEVELOPMENT LABS INC COSTA MESA CA  
INVESTIGATION OF THE RAYLEIGH CRITICAL ANGLE PHENOMENON FOR THE--ETC(U)  
APR 82 B P HILDEBRAND, G L FITZPATRICK F49620-81-C-0040  
UNCLASSIFIED AFOSR-TR-82-056A NL

1 OF 1  
ADA  
172 64



END  
DATE FILMED  
08-82  
DTIC

AD A117264

INVESTIGATION OF THE RAYLEIGH CRITICAL ANGLE PHENOMENON  
FOR THE CHARACTERIZATION OF SURFACE PROPERTIES

PHASE I

FINAL REPORT

April 1982

SDL No. 82-2188-07F

Principal Investigator  
B. P. Hildebrand

Senior Scientist  
G. L. Fitzpatrick

Computer Scientist  
A. J. Boland

Sponsored by:

Advanced Research Projects Agency (DOD)  
ARPA Order No. 4109

Monitored by AFOSR Under Contract #F49620-81-C-0040

"The views and conclusions contained in this document are those of the authors and should not be interpreted as necessarily representing the official policies, either expressed or implied, of the Defense Advanced Research Projects Agency or the U.S. Government."

**SPECTRON  
DEVELOPMENT  
LABORATORIES  
INC.**



AIR FORCE OFFICE OF SCIENTIFIC RESEARCH (AFSC)  
NOTICE OF TRANSMISSION TO DTIC  
This technical report has been reviewed and is  
approved for public release under the DODIA 130-12.  
Distribution is unlimited.  
MATTHEW J. KRAMER

3303 Harbor Boulevard, SMC/DTIC Technical Information Division  
Costa Mesa, California 92626 (714) 549-8477

A

**UNCLASSIFIED**

SECURITY CLASSIFICATION OF THIS PAGE (When Data Entered)

REPORT DOCUMENTATION PAGE			READ INSTRUCTIONS BEFORE COMPLETING FORM
1. REPORT NUMBER <b>AFOSR-TR- 82-0568</b>	2. GOVT ACCESSION NO. <b>AD-A111 264</b>	3. RECIPIENT'S CATALOG NUMBER	
4. TITLE (and Subtitle) INVESTIGATION OF THE RAYLEIGH CRITICAL ANGLE PHENOMENON FOR THE CHARACTERIZATION OF SURFACE PROPERTIES		5. TYPE OF REPORT & PERIOD COVERED FINAL - March 81 - April 82	
7. AUTHOR(s) B. P. Hildebrand, G. L. Fitzpatrick and A. J. Boland		6. PERFORMING ORG. REPORT NUMBER F49620-81-C-0040	
9. PERFORMING ORGANIZATION NAME AND ADDRESS Spectron Development Laboratories Inc. 3303 Harbor Boulevard, Suite G-3 Costa Mesa, CA 92626		10. PROGRAM ELEMENT, PROJECT, TASK AREA & WORK UNIT NUMBERS <b>6110-2F</b> <b>2306/A2</b>	
11. CONTROLLING OFFICE NAME AND ADDRESS Air Force Office of Scientific Research Bldg. 410 Bolling Air Force Base Washington, D.C. 20332		12. REPORT DATE 14 April 82	
14. MONITORING AGENCY NAME & ADDRESS (if different from Controlling Office)		13. NUMBER OF PAGES 70	
16. DISTRIBUTION STATEMENT (of this Report)  <i>Approved for public release, distribution unlimited.</i>		15. SECURITY CLASS. (of this report) <b>UNCLASSIFIED</b>	
17. DISTRIBUTION STATEMENT (of the abstract entered in Block 20, if different from Report)			
18. SUPPLEMENTARY NOTES  <i>SELECTED</i> <b>JUL 20 1982</b> <b>A</b>			
19. KEY WORDS (Continue on reverse side if necessary and identify by block number)  <b>NDE, critical angle, ultrasonics</b>			
20. ABSTRACT (Continue on reverse side if necessary and identify by block number)  An automated, computer controlled goniometer was constructed and perfected. Controlled measurements on a variety of materials, including materials of interest to the NDT community, were carried out and compared with theoretical predictions made by a number of authors. Experimental results indicate that these theories may be only first approximations to reality. A number of significant experimental anomalies, such as the appearance of more than one amplitude dip were found. Certain theoretical questions were raised regarding			

DD FORM 1 JAN 73 EDITION OF 1 NOV 65 IS OBSOLETE

**UNCLASSIFIED**

SECURITY CLASSIFICATION OF THIS PAGE (When Data Entered)

SECURITY CLASSIFICATION OF THIS PAGE(When Data Entered)

these theories including the question of momentum conservation at the interface. Both the experimental and theoretical observations suggest that modifications to existing theory may be necessary.

SECURITY CLASSIFICATION OF THIS PAGE(When Data Entered)

## TABLE OF CONTENTS

<u>No.</u>		<u>Page</u>
	TABLE OF CONTENTS . . . . .	1
	LIST OF FIGURES . . . . .	iii
	LIST OF TABLES . . . . .	vii
	ABSTRACT . . . . .	viii
1.0	INTRODUCTION AND BACKGROUND . . . . .	1
2.0	REVIEW OF PHASE I PLANS . . . . .	8
	2.1 Year I Tasks as Planned . . . . .	8
3.0	PROGRESS TOWARD ACHIEVING GOALS . . . . .	10
	3.1 Description of Apparatus . . . . .	10
	3.2 Computer Hardware . . . . .	14
	3.3 Set Up Procedures . . . . .	14
	3.4 The Automated Measuring System . . . . .	15
	3.5 Literature Search . . . . .	21
4.0	SUMMARY OF RESEARCH RESULTS (PHASE I) . . . . .	23
	4.1 Samples . . . . .	23
	4.2 Temperature Control . . . . .	24
	4.3 Experimental Procedure . . . . .	24
	4.4 Qualitative Features of Experimental Data . .	28
	4.5 Results and Anomalies . . . . .	29
	4.6 Frequency of Least Reflection (FLR) . . . . .	42
5.0	PROSPECTS FOR COMPARISON OF EXPERIMENTS WITH EXISTING THEORIES . . . . .	43
	5.1 The Richardson Model . . . . .	43

TABLE OF CONTENTS (CON'T)

<u>No.</u>		<u>Page</u>
5.2	The Model of Pitts . . . . .	48
5.3	Comparison of Pitts' and Richardson's Model . . . . .	52
5.4	Theoretical Difficulties . . . . .	53
5.5	Some Possible Remedies . . . . .	57
6.0	BRIEF REVIEW OF PHASE II PLANS . . . . .	61
7.0	SUMMARY AND CONCLUSIONS . . . . .	64
	ACKNOWLEDGMENTS . . . . .	65
8.0	REFERENCES . . . . .	66
9.0	SUPPLEMENTARY REFERENCES . . . . .	69
	APPENDIX A: FUNDAMENTAL BASIS FOR NONLINEAR NATURE OF ELASTIC WAVES . . . . .	A1

LIST OF FIGURES

<u>No.</u>		<u>Page</u>
1	THE EXPERIMENTAL SYSTEM FOR MAKING MEASUREMENTS OF $R(\theta)$ AND $\phi(\theta)$ VS $\theta$ CONSISTS OF A GONIOMETER IN FIGURE 1(a), AND A GIMBALED SAMPLE HOLDER IN FIGURE 1(b). THE COMPUTER CONTROLLED AUTOMATED SYSTEM IS SHOWN IN FIGURE 1(c) AND 1(d). DATA IS STORED ON DISC FOR ARCHIVAL PURPOSES AND MAY BE DISPLAYED AS SHOWN IN FIGURE 1(c). THE SYSTEM IS COMPATIBLE WITH PDP 11/23, APPLE, OR IBM PERSONAL COMPUTERS. WHEN x-y SCANNING IS PERFORMED, THE GIMBALED SAMPLE HOLDER IS REPLACED BY A SAMPLE MOUNT THAT CAN BE SCANNED. SCHEMATIC DIAGRAMS SHOWING THE APPARATUS AND SUPPORT ELECTRONICS ARE PROVIDED IN FIGURE 2. THE SYSTEM IS IMMersed IN A SMALL WATER TANK (NOT SHOWN) TO ACHIEVE ACOUSTIC COUPLING TO THE SAMPLE. . . . .	11
2	THIS FIGURE ILLUSTRATES THE SUPPORT EQUIPMENT AND GENERAL FUNCTION FOR THE x-y SCANNING SYSTEM. THIS SYSTEM PRODUCES IMAGES OF $R(\theta)$ AND $\phi(\theta)$ AT A FIXED $\theta$ . WE CAN ALSO PRODUCE CURVES OF $R(\theta)$ AND $\phi(\theta)$ VERSUS $\theta$ . . . . .	16
2	(CONTINUED). SCHEMATIC DIAGRAM SHOWING APPARATUS USED TO MEASURE THE REFLECTED AMPLITUDE $R(\theta)$ AND THE PHASE $\phi(\theta)$ OF THE REFLECTED WAVE. THE SYSTEM ALLOWS ONE TO PERFORM AUTOMATED COMPUTER CONTROLLED MEASUREMENTS AND DISPLAY THEM ON A CRT MONITOR . . .	17
3	TYPICAL EXPERIMENTAL CURVES FOR ALUMINUM. $R(\theta)$ IS THE REFLECTED AMPLITUDE VS INCIDENT ANGLE $\theta$ . $\phi(\theta)$ IS THE PHASE OF THE REFLECTED WAVE. THE CRITICAL ANGLE FOR SURFACE WAVE GENERATION OCCURS HERE AT ABOUT $32^\circ$ . . . . .	19
4	A FLAT BOTTOMED 1/4 INCH DIAMETER HOLE WITHIN 1/32 INCH OF THE SURFACE IN ALUMINUM IS IMAGED IN THE x-y SCANNING MODE (SEE FIGURE 2). AT THE CRITICAL ANGLE $\theta = \theta_{cr}$ , THE HOLE IS VISIBLE IN BOTH PHASE $\phi(\theta)$ AND AMPLITUDE $R(\theta)$ PLOTS. THIS ILLUSTRATES THAT A SURFACE WAVE IS GENERATED AT $\theta = \theta_{cr}$ . . . . .	19
5	AN EXAMPLE OF COMPUTER GENERATED REFLECTION FACTORS $R(\theta)$ AND PHASE $\phi(\theta)$ VS. THE INCIDENT ANGLE $\theta$ FOR TWO CASES OF ATTENUATION $\alpha$ IN THE SOLID. $\alpha_1 > \alpha_2 \approx 0$ . THE ALGORITHM USED WAS OBTAINED FROM R. L. RICHARDSON	20

LIST OF FIGURES (CON'T)

<u>No.</u>		<u>Page</u>
6	TEMPERATURE EFFECTS. A SAMPLE OF TITANIUM WAS EXAMINED AT A SERIES OF TEMPERATURES RANGING FROM 5 TO 25°C. STRAINS IN THE APPARATUS AND CHANGES IN VELOCITY IN BOTH THE WATER BATH AND THE SPECIMEN CONTRIBUTE TO CHANGES IN THE CRITICAL ANGLE $\theta_c$ . IT IS CLEAR THAT TEMPERATURE VARIATIONS ARE IMPORTANT IN SUCH MEASUREMENTS SINCE WE OBSERVE A CHANGE OF APPROXIMATELY 1° IN $\theta_c$ FOR 5°C (BETWEEN 10 - 15°C) CHANGE IN TEMERATURE. . . . .	25
7	REPRODUCIBILITY OF MEASUREMENTS. AN ALUMINUM SAMPLE WAS MAINTAINED AT 25°C AND MEASUREMENTS OF $\theta_c$ WERE MADE OVER A PERIOD OF HOURS. A NUMBER OF MEASUREMENTS WERE ALSO MADE AFTER REPEATEDLY REPLACING AND REMOVING THE SAMPLE. THESE MEASUREMENTS (NOT SHOWN) HAD ESSENTIALLY THE SAME ERROR AS THE SAMPLE THAT WAS NOT REMOVED DURING THE SERIES OF MEASUREMENTS. . . . .	26
8	SCHEMATIC DIAGRAM OF A TYPICAL EXPERIMENTAL CURVE FOR THE REFLECTED AMPLITUDE $R(\theta)$ AND PHASE $\phi(\theta)$ OF THE REFLECTED WAVE. . . . .	30
9	EXPERIMENTAL ARRANGEMENT OF THE SOURCE AND RECEIVER	30
10	EXPERIMENTAL MEASUREMENTS ON A TITANIUM ALLOY AT 3.1 MHZ (25°C) SHOWING THE REFLECTED AMPLITUDE (RELATIVE UNITS) $R(\theta)$ IN THE UPPER CURVE AND THE PHASE $\phi(\theta)$ LOWER CURVE. IN THESE CURVES, THE TIC MARKS ARE 2° AND THE RANGE OF THE PHASE DATA IS 360°. THE DATA AT THE RIGHT SUPPLIES FURTHER INFORMATION REGARDING THE SPECIMEN. . . . .	31
11	SAME SPECIMEN AS SHOWN IN FIGURE 10, BUT WITH A BETTER MINIMUM IN $R(\theta)$ . DISTORTIONS IN THE PHASE CURVE $\phi(\theta)$ (BOTTOM CURVE) ARE READILY APPARENT. . .	31
12	SCHEMATIC DIAGRAM SHOWING THE OBSERVED SIGNAL AT THE MINIMUM OF $R(\theta)$ . THIS SIGNAL APPEARS TO BE THE SUM OF A PRIMARY WAVE OF FREQUENCY $\omega_0$ AND A SECOND HARMONIC FREQUENCY $2\omega_0$ AT 90° TO THE PRIMARY. WHENEVER SUCH A SIGNAL WAS OBSERVED, THE PHASE CURVES WERE INVARIABLY DISTORTED. HOWEVER,	

LIST OF FIGURES (CON'T)

<u>No.</u>		<u>Page</u>
	IT WAS SOON LEARNED THAT THIS SECOND HARMONIC CONTAMINATION WAS NOT RESPONSIBLE FOR THESE DISTORTIONS SINCE THE PHASE METER DID NOT RESPOND TO THIS COMPONENT (SEE TEXT FOR A DISCUSSION). . . . .	34
13	MATERIALS SHOWING MULTIPLE AMPLITUDE DIPS. IN (a) A TITANIUM SPECIMEN SHOWING TWO DIPS AND TWO DISTORTED PHASE SHIFTS IS REPRODUCED. THE TWO DIPS ARE SEPARATED BY ROUGHLY $3^\circ$ . SIMILARLY, IN (b) A CALCIUM FLUORIDE CRYSTAL SHOWS TWO AMPLITUDE DIPS SEPARATED BY ABOUT $4^\circ$ . FINALLY, IN (c) AND (d) WE ILLUSTRATE TWO MEASUREMENTS (ONE AUTOMATED AND THE OTHER A HAND MEASUREMENT) ON A 4340 STEEL SPECIMEN. IN THE HAND MEASURED CURVE, THERE ARE CLEARLY TWO DIPS. INDICATIONS OF A THIRD AMPLITUDE DIP APPEAR IN THE AUTOMATED MEASUREMENT. . . . .	37
14	THE CONVENTIONAL ANALYSIS OF THE REFLECTION AND TRANSMISSION COEFFICIENTS OF A LIQUID-SOLID BOUNDARY UP TO THE SHEAR CRITICAL ANGLE $\theta_s$ . CURVES TAKEN FROM BREKHOVSKIKH. <sup>1</sup> $\theta_L$ IS THE LONGITUDINAL CRITICAL ANGLE. IN THE LOSSLESS CASE, ENERGY IS CONSERVED AND $E = E' + E_t + E_\ell$ . TOTAL REFLECTION OCCURS AT $\theta_L$ AND $\theta_s$ . . . . .	55
15	A TOTALLY REFLECTED SOUND WAVE. HOW IS THE MOMENTUM TRANSFERRED TO THE SOLID EVEN IF ENERGY IS CONSERVED? . . . . .	56
16	THIS FIGURE ILLUSTRATES THE CONVENTIONAL PARTITIONING OF AN INCIDENT WAVE INTO A RESPONDENT "LEAKY" SURFACE WAVE AT THE CRITICAL ANGLE AND REFLECTED AND RERADIATED COMPONENTS. ONE CAN EASILY IMAGINE THAT MOMENTUM IS CONSERVED ALONG X BUT UNLESS THERE IS A BULK WAVE IN THE SOLID, HOW CAN IT BE CONSERVED ALONG Z? IF THERE ARE NO BULK WAVES IN THE SOLID, WE HAVE THE ADDED PROBLEM OF AN UNCOMPENSATED COUPLE (ANGULAR MOMENTUM) DUE TO THE DISPLACEMENT OF THE RERADIATED WAVE . . . .	62

LIST OF FIGURES (CON'T)

<u>No.</u>		<u>Page</u>
17	THE CRITICAL ANGLE MEASURING SYSTEM CURRENTLY BEING USED EMPLOYS A POINT DETECTOR AT R <sub>1</sub> AND A LENS SOURCE AT S. IN THE MODIFIED ARRANGEMENT, WE INTEND TO PLACE A FOCUSED DETECTOR (SAME AS S) AT R <sub>2</sub> . WE WILL USE THIS TO EXAMINE ANY ISOTROPIC RADIATION COMPONENT FROM THE REGION TO THE "POINT" FOCUS. . . . .	63

LIST OF TABLES

<u>No.</u>		<u>Page</u>
1	PRINCIPAL CRITICAL ANGLE $\theta_c$ FOR VARIOUS MATERIALS AT THE FREQUENCY OF LEAST REFLECT FLR . . . . .	40

## ABSTRACT

The Phase I study of the "Rayleigh" critical angle phenomenon has been completed. An automated, computer controlled goniometer was constructed and perfected. Controlled measurements on a variety of materials, including materials of interest to the NDT community, were carried out and compared with theoretical predictions made by a number of authors.

Experimental results indicate that these theories are only first approximations to reality. We find a number of significant experimental anomalies, such as the appearance of more than one amplitude dip. Certain theoretical questions can also be raised regarding these theories including the question of momentum conservation at the interface. Both the experimental and theoretical observations suggest that we are not yet in possession of a complete theory.

Phase II plans are designed to investigate both experimentally and theoretically these questions so that our goal of a better theoretical understanding of this phenomenon can be achieved. Given this improved understanding, practical quantitative NDT techniques based on the "Rayleigh" critical angle phenomenon will become available.

## 1.0 INTRODUCTION AND BACKGROUND

The introduction of high performance machines, such as aircraft engines and gas turbines, demands increasingly exotic materials capable of handling high temperature and stress. These materials are generally of the ceramic or super alloy type formed by powder metallurgy. Since these materials are intended to operate under severe environments, it is important to be able to characterize them as much as possible. Such parameters as grain size, residual stress, and number and size of defects have an important bearing on the machinability and performance of any component fabricated from the material. Thus, there is a need for methods to perform a nondestructive evaluation of these materials.

Current methods for nondestructive evaluation of materials include x-ray, eddy current, dye penetrant, and ultrasonics. All of these techniques have advantages and disadvantages. One of the most popular methods is ultrasonic, used in the pulse-echo mode. This method sends pulses of ultrasound into the material and examines the echos returned from within. The size of internal defects is estimated by analyzing the echos. It is also possible to create images by scanning the transducer over the material surface, and recording the echos in their correct spatial position.

Ultrasonic inspection has several disadvantages when applied to the new materials. One of the major problems is the inability to resolve near-surface defects due to ringing and reverberation

phenomena. The other major problem is a lack of resolution (on the order of 1 mm). For critical components, near-surface defects are the most important since fractures occurring at the surface will cause rapid deterioration and can lead to catastrophic failure at the high temperatures and pressures which must be endured. In addition, current ultrasonic methods are incapable of measuring grain size and surface residual stress which also influence material behavior.

The purpose of the research reported here is to investigate the feasibility of harnessing a nearly unused phenomenon of ultrasound, the so-called Rayleigh critical angle effect, to provide measurement of grain size, defect location and size, and surface residual stress distribution to name a few. If feasibility can be established, the way is open to the development of inspection instrumentation capable of evaluation materials as they come from the production line.

It is well known that an ultrasonic wave propagating from one medium to another undergoes significant alteration at the boundary.<sup>1-3</sup> When a wave propagates from a liquid into a solid, three new waves generally appear; one reflected and two propagated. The propagated waves travel at angles defined by Snell's law, and the reflected wave obeys the law of reflection.<sup>4</sup> Specifically, the direction of the propagated bulk longitudinal wave is given by:

$$\sin \theta_{12} = \frac{v_{12}}{v_{11}} \sin \theta_{11}, \quad (1)$$

the propagated bulk shear wave angle by:

$$\sin \theta_{22} = \frac{v_{22}}{v_{11}} \sin \theta_{11}, \quad (2)$$

and the reflected wave angle by:

$$\theta_{1r} = \theta_{11} \quad (3)$$

where  $v_{11}$  = velocity of longitudinal waves in liquid,

$v_{12}$  = velocity of longitudinal waves in solid,

$v_{22}$  = velocity of shear waves in solid, and

$\theta_{11}$  = angle of incidence.

The above equations hold for ideal media having no attenuation.

When attenuation is present, Snell's law becomes more complicated since velocity and/or wave number now becomes a complex quantity.<sup>5</sup>

Snell's law predicts the interesting phenomenon known as the critical angle. This is easily seen from an examination of equations 1 and 2. At some incident angle, the angle of refraction of either the longitudinal or shear wave becomes 90° indicating that one or both of these refracted waves no longer exist in the material. Typically, for steel, the longitudinal critical angle occurs at about 17°, and the shear critical angle occurs at about 31°. The simple equations predict no more than this. In fact, the classical theory for the behavior of sound predicts complete

reflection at and beyond the shear critical angle.

Experiments show, however, that the behavior just beyond the shear critical angle is much different than predicted by classical theory.<sup>6-8</sup> The amplitude of the reflected wave dips sharply just beyond the shear critical angle and its phase undergoes a relatively large shift, typically 360°. It is observed that just beyond (approximately 1°) the shear critical angle a Rayleigh-type surface wave is set up on the liquid-solid boundary. Obviously, the theory must be modified to account for this behavior. This has been done by several authors<sup>9-16</sup> who have introduced attenuation in this problem. This results in a new reflection coefficient.

The models seem to predict observed behavior for unbounded beams with good accuracy.<sup>11</sup> Both the dip in amplitude and the phase change seem to be predicted quantitatively as well as qualitatively in cases where it has been experimentally tested. Such unbounded beam theories have also been extended to include the case of bounded beams which leads to further insights into experimental observations.

In addition to describing the behavior of the reflected wave at the critical angle, these theories indicate that there should exist a frequency at which there is zero reflection at the critical angle, called the frequency of least reflection (FLR). This point is apparently dependent upon grain size, and appears to present a method for its measurement. The theory of Richardson<sup>13</sup> also seems

to predict that grain size could be measured to a resolution on the order of  $0.2 \mu\text{m}$  by measuring the FLR to 0.1%.<sup>16</sup>

In the course of the experimental verification, some interesting transient effects were observed by several authors.<sup>17</sup> It was noted that the phase response near the critical angle involved a time lag. That is, it took a finite amount of time after initiation of the ultrasonic burst before the phase of the reflected wave changed from the classically predicted value to that obtained with the steady state theories. It is speculated that this time delay may be a measure of the viscous properties of the material. Thus, it appears that extension of these theories to include transient effects might be profitable.

Any changes that affect attenuation and velocity can be detected by the behavior of the reflected wave at the critical angle. Some general statements can be made about these effects.

- 1) The depth of the reflectivity minimum depends on attenuation, principally that of the shear wave although the phase shift is insensitive to changes in shear wave attenuation.
- 2) Angular position of the surface wave critical angle depends on velocity, principally that of the shear wave.
- 3) The two effects listed above appear to be independent.
- 4) Changes in critical angle with frequency probably result from velocity gradients with depth.

The critical angle phenomenon is, however, a near surface effect extending into the material to a distance of roughly the wavelength of surface waves. Thus, the selection of frequency

could be used to probe different near-surface layers. For example, it may be possible to measure the stress distribution in the solid as a function of depth by tracking the critical angle as a function of frequency. Martin has shown that the surface wave velocity can be measured by monitoring the critical angle with sufficient accuracy to enable discrimination of  $3.3 \times 10^5$  dyn/cm<sup>2</sup> uniaxial stress.<sup>17-19</sup> By starting at a high frequency and progressing to lower frequencies, the stress variation with depth could be analyzed layer by layer.

There are a variety of ways in which the critical angle phenomenon could be used to produce images. Among these are:

- A. Plot of critical angle versus position,
- B. Plot of the FLR at the critical angle versus position,
- C. Plot of amplitude of the reflected wave for fixed angle of incidence at the nominal critical angle versus position, and
- D. Plot of phase of the reflected wave for fixed angle of incidence at the nominal critical angle versus position.

The various imaging modes listed above (A, B, C, D) would be sensitive to different combinations of material properties as indicated below:

Mode A: Material "variation" and/or surface stress

Mode B: Grain size

Mode C: Grain size, surface stress, material variation, and

Mode D: Material variation and/or surface stress

Material variation may consist of changes in hardness, presence of

defects, changes in chemical composition, etc.; in general, anything that causes local variation of the shear wave velocity.

Only one known experiment in critical angle imaging has been reported.<sup>20</sup> In this experiment, method D was used to image a hardness variation and a subsurface defect with excellent results. The possibilities discussed above are only the obvious ones based on the results available at this time. Other applications will arise as more work is done.

In the present report, the results of both experimental and theoretical studies of this problem are presented. Certain anomalous results and various theoretical difficulties suggest that the correct theoretical description is not yet available. Studies are proposed to remedy these deficiencies.

## 2.0 REVIEW OF PHASE I PLANS

There were five principal tasks outlined in the original proposal for the first year's work.

### 2.1 Year I Tasks As Planned

In brief these tasks were:

#### Task 1 - Theoretical Review of Steady State Theory

The theories of Richardson,<sup>13</sup> Merkulova,<sup>15</sup> and Bertoni and Tamir,<sup>21-23</sup> will be reviewed and combined to provide the most complete picture of the critical angle phenomenon possible. As well, a search of the modern literature will be made to ascertain that no new theories have been proposed since their work. The Russian literature, in particular, will be carefully perused since much theoretical work is going on there. At the end of this task, the steady state theory should be firmly established and ready for exploitation.

#### Task 2 - Experimental Backup for Task 1

A precision goniometer will be designed and fabricated so that precise critical angle measurements may be made. A system consisting of the goniometer, transducers, ultrasonic generator, and measurement instruments such as a vector voltmeter will be assembled. With the advice of the Materials Research Center of the NBS, a number of flat samples of well characterized materials, such as AL 6061-T6, will be obtained. These will be completely characterized (with respect to the critical angle parameters) by recording the phase and amplitude of the reflected wave versus angle with frequency as a parameter. From these curves other curves may be derived. These are critical angle versus frequency, amplitude minimum at the critical angle versus frequency, width of amplitude dip around the critical angle versus frequency, and slope of phase change at the critical angle versus frequency. From these derived curves, certain characteristics of the material can be established. These are amplitude and frequency of least reflection, frequency of narrowest amplitude dip, and frequency of largest phase slope. It is expected that the frequencies should all be the same.

The ultrasonic parameters of the sample, velocity, and attenuation of the longitudinal and shear waves would be inserted into the theory and the same theoretical curves drawn.

Thus, Task 2 would provide a thorough comparison of theory and practice.

#### Task 3 - Development of Transient Theory

The theory reviewed and revised in Task 1 would be extended to include the transient case. It is suspected that the time lag to steady state behavior may be an additional and independent variable useful in characterizing the material.

#### Task 4 - Experimental Backup for Task 3

The same samples and measurement system developed in Task 2 would be used to verify the transient theory. Instead of continuous wave signals, step functions (gated sine waves) would be used with careful attention paid to the time interval before steady state response is achieved. Since at this time it is not known exactly what to expect, a particular set of experiments cannot be specified.

#### Task 5 - Applications Experiments

Since it is already established that subsurface flaws can be detected by the phase shift at the critical angle, this application will be investigated first. A sample, similar to those used in Tasks 2 and 4, will be prepared by drilling flat-bottomed holes into it. These holes will be arranged in specific patterns of size, distance from the surface, and separation. The goniometer will be mounted on an x-y scanner so that a two-dimensional distribution of critical angle parameters may be detected and displayed. In this way, resolution and sensitivity of the various parameters to the flaw can be ascertained.

### 3.0 PROGRESS TOWARD ACHIEVING GOALS

In the course of making acoustic critical angle measurements early in the program, it gradually became obvious that a better experimental apparatus was needed. Great difficulty was experienced in leveling and orienting samples. Sample surfaces were often found to be too rough or insufficiently flat to obtain reproducible measurements and it was also determined that results are temperature dependent. Measurements made at different times were often not repeatable owing to unknown temperatures.

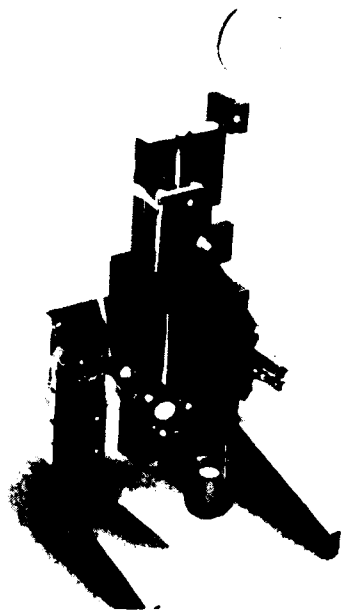
These difficulties have been overcome by incorporating a gimbaled sample holder (see Figure 1), and employing a temperature controlled bath. We have also obtained a grinding lap for producing flat samples with uniform surface characteristics.

#### 3.1 Description of Apparatus

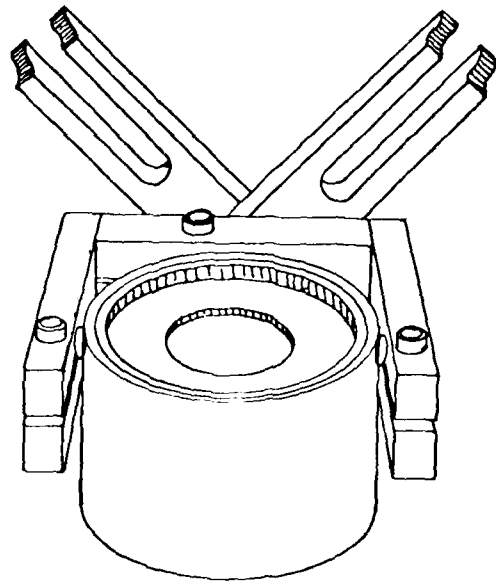
A gimbaled sample holder (Figure 1) was designed and constructed. This device, which is patterned after a microscope mirror mount, is designed to accept samples measuring not more than two inches in maximum dimension and possessing at least one flat surface.

The sample holder is fitted with a threaded ring and various disc "windows" for adapting to samples of different sizes and shapes. Not only can the orientation of the plane sample surface be changed, but the elevation may also be changed by slight adjustments of the rings. With this new device in place, most of the former

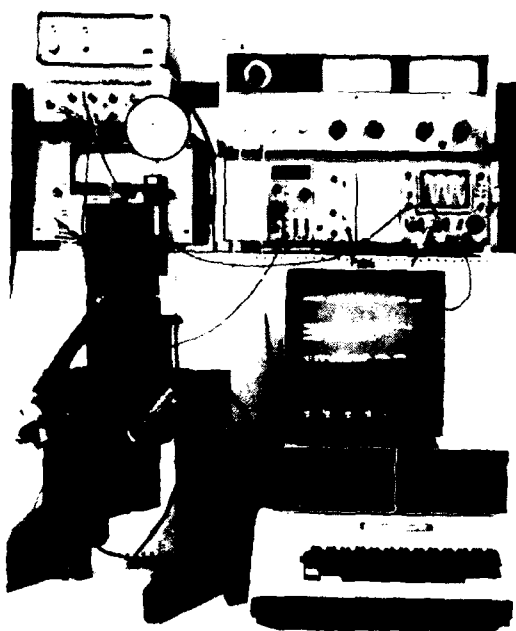
FIGURE 1. THE EXPERIMENTAL SYSTEM FOR MAKING MEASUREMENTS OF  $R(\theta)$  AND  $\phi(\theta)$  VS  $\theta$  CONSISTS OF A CONIOMETER IN FIGURE 1(a), AND A GIMBALED SAMPLE HOLDER IN FIGURE 1(b). THE COMPUTER CONTROLLED AUTOMATED SYSTEM IS SHOWN IN FIGURE 1(c) AND 1(d). DATA IS STORED ON DISC FOR ARCHIVAL PURPOSES AND MAY BE DISPLAYED AS SHOWN IN FIGURE 1(c). THE SYSTEM IS COMPATIBLE WITH PDP 11/23, APPLE, OR IBM PERSONAL COMPUTERS. WHEN x-y SCANNING IS PERFORMED, THE GIMBALED SAMPLE HOLDER IS REPLACED BY A SAMPLE MOUNT THAT CAN BE SCANNED. SCHEMATIC DIAGRAMS SHOWING THE APPARATUS AND SUPPORT ELECTRONICS ARE PROVIDED IN FIGURE 2. THE SYSTEM IS IMMersed IN A SMALL WATER TANK (NOT SHOWN) TO ACHIEVE ACOUSTIC COUPLING TO THE SAMPLE.



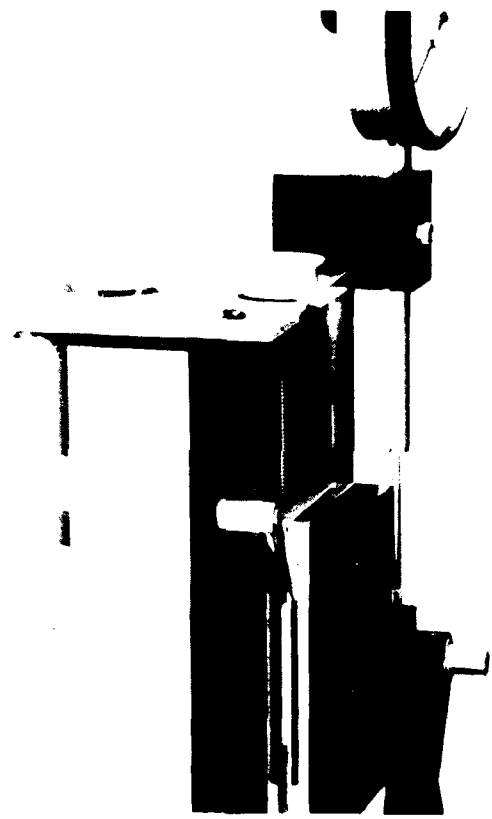
1(a) CONIOMETER AND SAMPLE HOLDER



1(b) SCHEMATIC OF GIMBALED SAMPLE HOLDER



1(c) COMPLETE SYSTEM



1(d) CLOSE-UP OF STEPPER MOTOR

problems with sample leveling and orienting have apparently been eliminated.

In addition to the gimbaled sample holder, several other minor mechanical improvements were made. The goniometer apparatus was fitted with leg mounts (see Figure 1), and a much smaller water tank was constructed. This reduced water volume allows the system to be placed on a lab bench, and also reduces problems that would be associated with maintaining a large volume of water at a fixed temperature.

### 3.2 Computer Hardware

One of the principal requirements of Phase I is to use a device of the foregoing type to obtain reliable data for assessing the validity of various theories of the critical angle phenomenon. Measurements of reflected amplitude  $R(\theta)$  and phase  $\delta(\theta)$  versus the angle of incidence  $\theta$  are required.

We have been using the PDP 11/23 computer system to make and store measured data using our automated measuring system. This computer is unnecessarily large for this task. Accordingly, we have made plans for adapting the system to a smaller computer. In Phase II we plan to employ an IBM personal computer instead of the PDP 11/23.

### 3.3 Set Up Procedures

With the new mechanical improvements in place, we have been

able to develop a simple set up procedure that allows one to make rapid and reliable measurements. Several tests of reproducibility involving the same and different observers and the same and different samples have been made. There are still effects, including possible nonlinear effects to be discussed, that may at times affect reliability. However, we feel that we now have the ability to make measurements that are sufficiently reliable so that we can begin to make meaningful comparisons between theory and experiment.

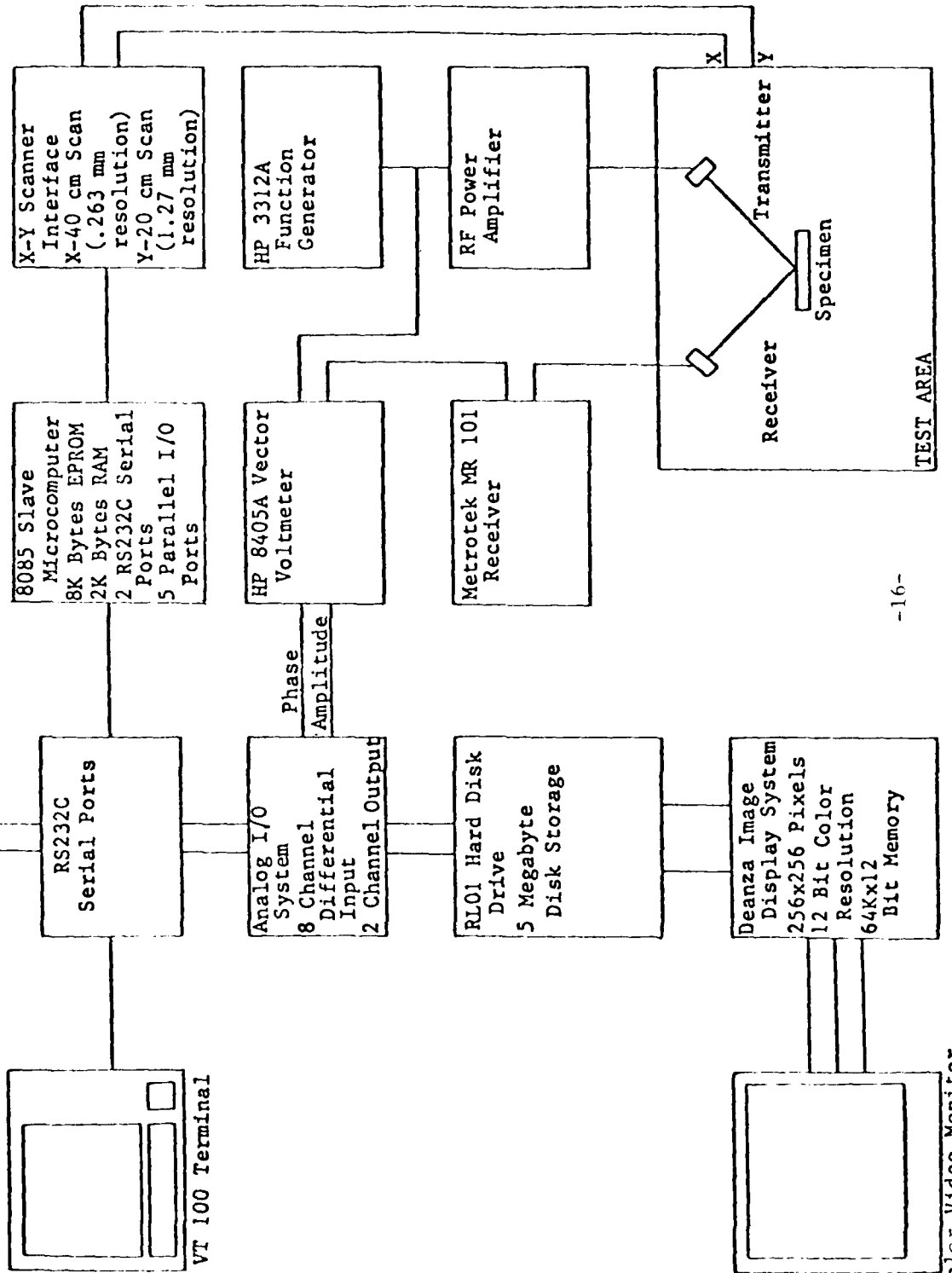
### 3.4     The Automated Measuring System

The original proposal called for the construction (Task 2) of a goniometer of unspecified design for making acoustic critical angle measurements. Not only was such a device constructed and the necessary auxiliary support equipment assembled (see Figures 1 and 2), but it has been converted to a computer-controlled automated measuring system. We may program the system to begin measurements at some initial angle of incidence  $\theta_i$  and continue in steps of  $\Delta\theta$  until a final angle  $\theta_f$  is reached.

Data is automatically analyzed to find the angle corresponding to the minimum reflection amplitude (the critical angle), and is displayed graphically (see Figure 3) on a CRT along with descriptive data regarding the experiment and the sample. The data is also stored on disc for archival purposes. The system allows us to make very accurate measurements of  $R(\theta)$  and  $\phi(\theta)$  in a rapid fashion. The computer-controlled system is also capable of operating in an

LSI 11/23  
 Microcomputer  
 64K Bytes RAM  
 High Speed  
 Arithmetic Chip  
 9 Quad Slot  
 Q-Buss Back  
 Plane

FIGURE 2. THIS FIGURE ILLUSTRATES THE SUPPORT EQUIPMENT  
 AND GENERAL FUNCTION FOR THE X-Y SCANNING  
 SYSTEM. THIS SYSTEM PRODUCES IMAGES OF R( $\epsilon$ )  
 AND  $\zeta(\theta)$  AT A FIXED  $\theta$ . WE CAN ALSO PRODUCE  
 CURVES OF R( $\theta$ ) AND  $\zeta(\theta)$  VERSUS  $\theta$ .



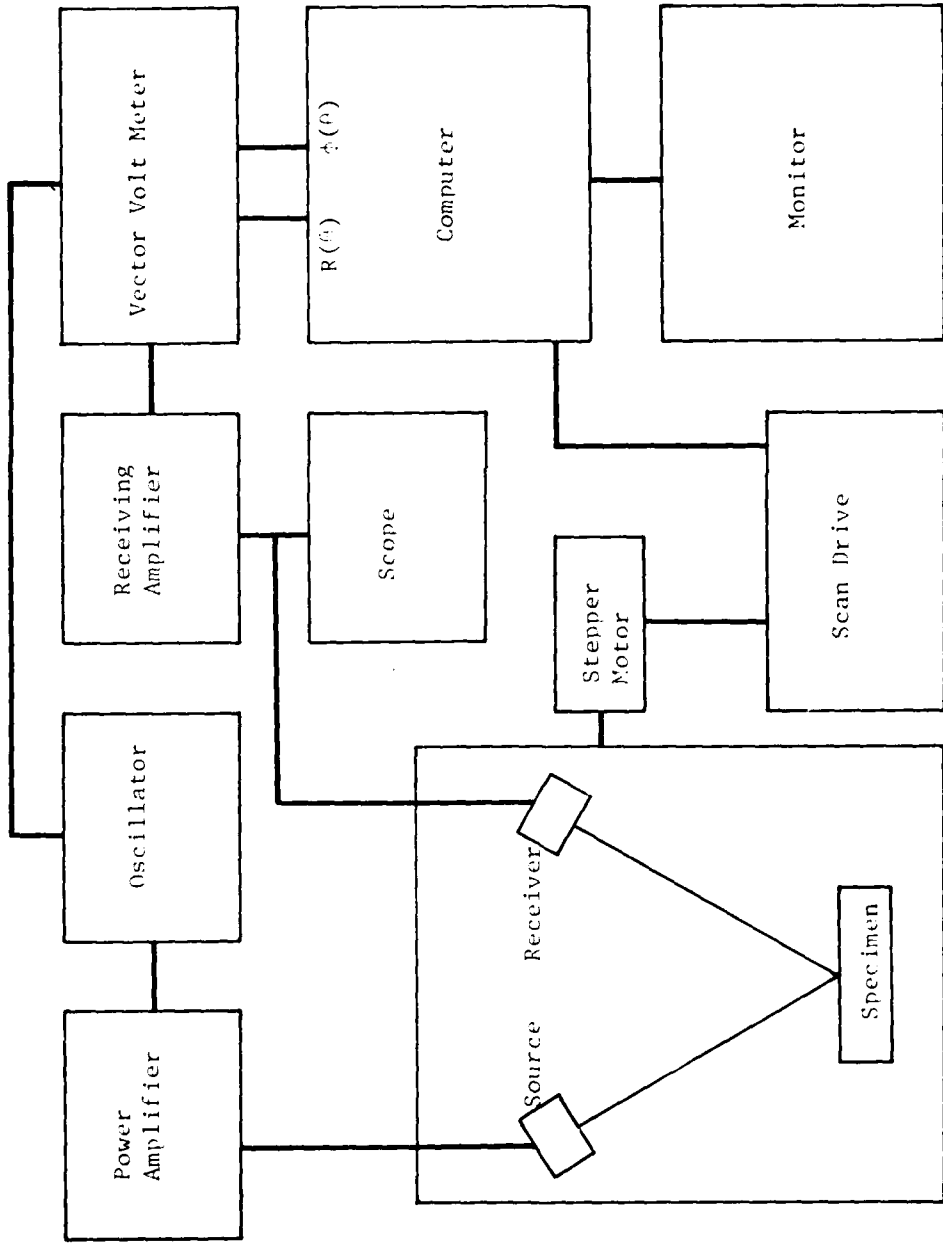


FIGURE 2 (Continued). SCHEMATIC DIAGRAM SHOWING APPARATI'S USED TO MEASURE THE REFLECTED AMPLITUDE  $R(t)$  AND THE PHASE  $\phi(t)$  OF THE REFLECTED WAVE. THE SYSTEM ALLOWS ONE TO PERFORM AUTOMATED COMPUTER CONTROLLED MEASUREMENTS AND DISPLAY THEM ON A CRT MONITOR.

x-y scanning mode: thereby, making possible "images" of the scattered wave at some fixed angle, usually the critical angle.

In Figure 4 we illustrate an example of the capability of our device to produce x-y scanned images of  $R(\theta)$  and/or  $\phi(\theta)$  at some fixed angle  $\theta$  (usually a critical angle). This capability (a Task 5 goal) has also been used on holes at varying depths; and it has been shown that by varying the frequency, the depth of penetration of the surface wave can be varied to determine the depths to such holes.

Part of Task 2 involved attempting to determine material parameters by fitting experimental data to the Richardson model. Accordingly, we have acquired a complete set of programs (courtesy of R. L. Richardson) which allows one to calculate the reflection coefficient  $R(\theta)$  and phase  $\phi(\theta)$  versus  $\theta$  where  $\theta$  is the angle of incidence of an unbounded longitudinal wave on a liquid-solid interface.

These programs were rewritten for use on our PDP 11/23 computer system and curves, such as that shown in Figure 5 for a stainless steel water interface, were computed and plotted. Various input parameters such as; material attenuation, shear wave velocity, and so on were chosen for these plots.

We hope eventually to be able to fit such curves to our experimental data; and thereby, infer the material parameters. Standing in the way of this are two problems. First, as mentioned elsewhere, we are not yet apparently in possession of a complete theory. Second, our method of measuring data involves a complex

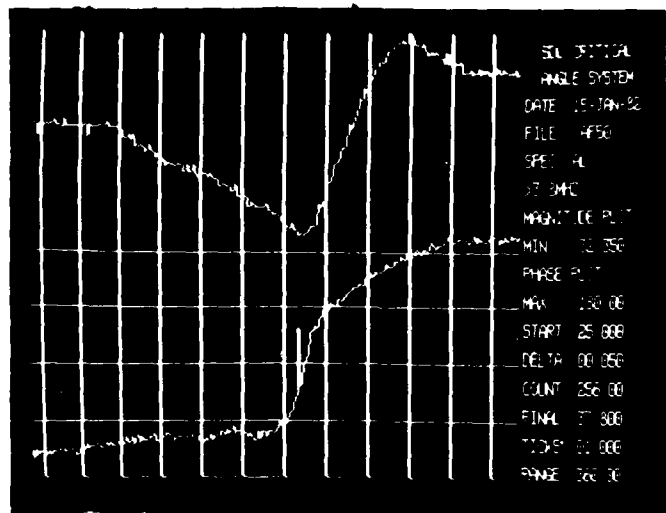


FIGURE 3. TYPICAL EXPERIMENTAL CURVES FOR ALUMINUM.  $R(\theta)$  IS THE REFLECTED AMPLITUDE VS INCIDENT ANGLE  $\theta$ .  $\phi(\theta)$  IS THE PHASE OF THE REFLECTED WAVE. THE CRITICAL ANGLE FOR SURFACE WAVE GENERATION OCCURS HERE AT ABOUT  $32^\circ$ .

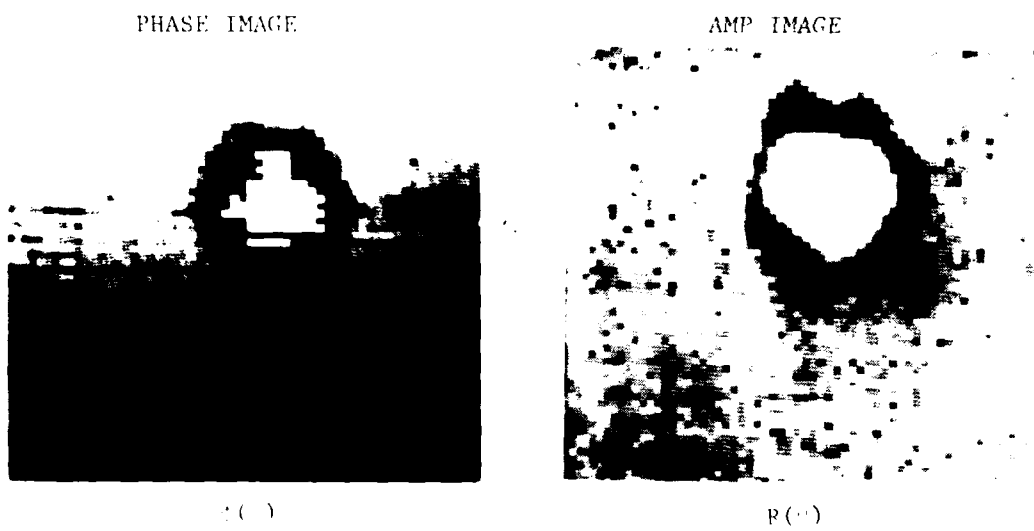


FIGURE 4. A FLAT BOTTOMED 1/4 INCH DIAMETER HOLE WITHIN 1/32 INCH OF THE SURFACE IN ALUMINUM IS IMAGED IN THE x-y SCANNING MODE (SEE FIGURE 2). AT THE CRITICAL ANGLE  $\theta = \theta_{cr}$ , THE HOLE IS VISIBLE IN BOTH PHASE  $\phi(\theta)$  AND AMPLITUDE  $R(\theta)$  PLOTS. THIS ILLUSTRATES THAT A SURFACE WAVE IS GENERATED AT  $\theta = \theta_{cr}$ .

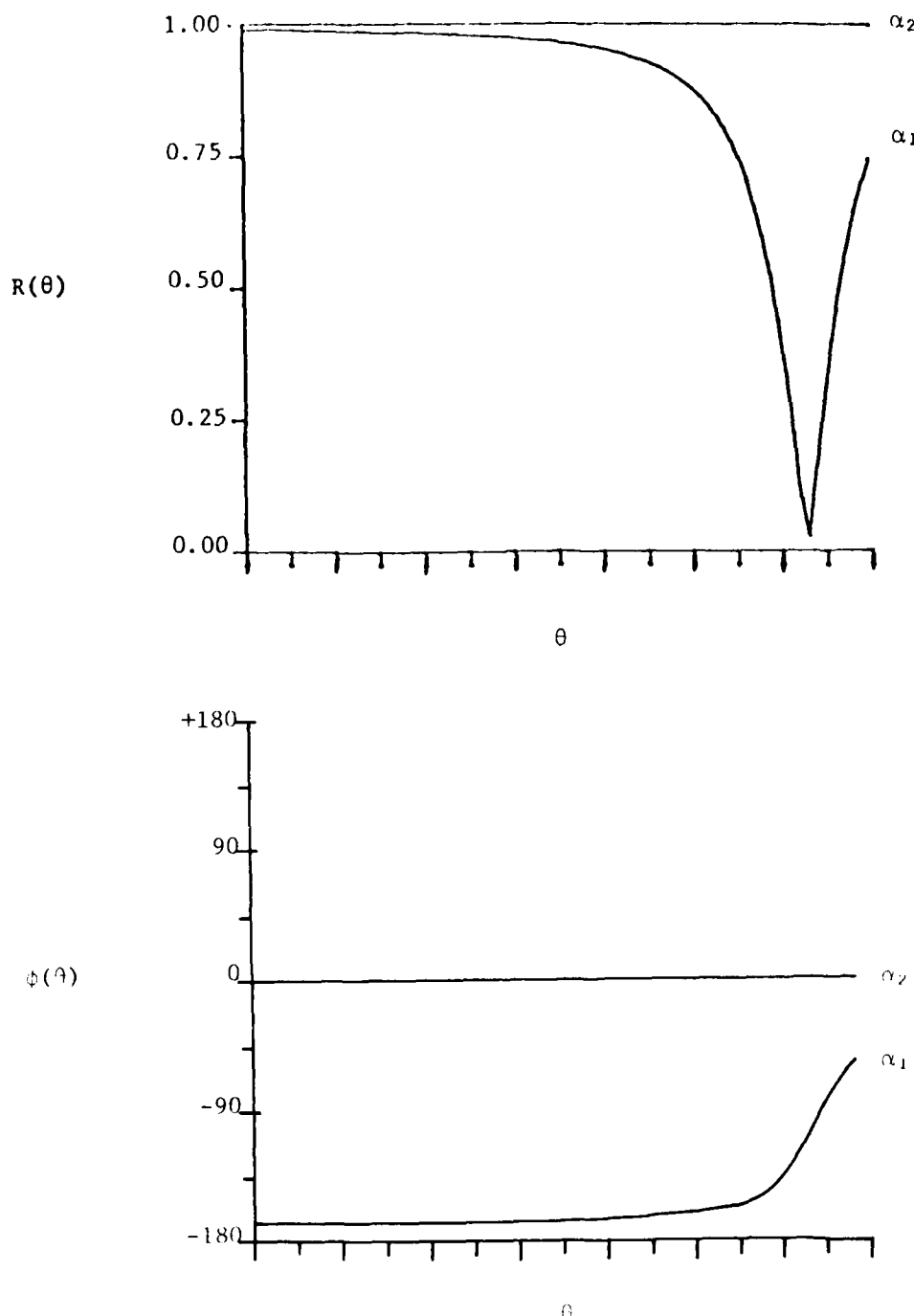


FIGURE 5. AN EXAMPLE OF COMPUTER GENERATED REFLECTION FACTORS  $R(\theta)$  AND PHASE  $\phi(\theta)$  VS. THE INCIDENT ANGLE  $\theta$  FOR TWO CASES OF ATTENUATION  $\alpha$  IN THE SOLID.  $\alpha_1 >> \alpha_2 \approx 0$ . THE ALGORITHM USED WAS OBTAINED FROM R. L. RICHARDSON.

bounded beam (spherical focused beam) rather than an unbounded beam (Richardson's programs cover this case).

Nevertheless, for many materials, curves of  $R(\theta)$  and  $\phi(\theta)$  versus  $\theta$  look qualitatively similar to those of Figure 5. Furthermore, although we use a complex bounded beam, we also employ a very narrow angle "point" detector which should see only one reflected wavevector (unless many wavevectors interact nonlinearly). All beam shift effects apparently occur at points sufficiently distant from our detector; that is, this single detected wavevector may well act like a reflected unbounded beam and should be comparable in many cases with Richardson's calculations. We will accordingly attempt to curve fit several well behaved experimental materials to the Richardson model; and thereby, fix the material parameters used in his model.

### 3.5 Literature Search

The goal of the Task 1 literature search was to study and compare works on bounded and unbounded acoustic beams as they influence the observed critical angle phenomenon.

Accordingly, the University of Washington information retrieval service among other sources was used to obtain references pertaining to the Rayleigh critical angle phenomenon and its applications. A search of three data bases was carried out. These were: A) COMPENDEX - January 1970-present, 935,688 records. Sources include 3500 journals, publications of engineering societies and

organizations, papers from proceedings of conferences and selected government reports, and books; B) INSPEC - 1969-present, 1,661,133 citations. Sources include Physics Abstracts, Electrical and Electronic Abstracts, and Computer and Control Abstracts; C) NTIS - 1964-present, 833,513 citations. Sources include government sponsored research, development, engineering plus analyses prepared by federal agencies, their contractors or grantees. Agencies such as NASA, DD, DOE, HEW, HUD, AND DOT are included. In addition, we have obtained a number of useful references from other published papers and from conversations with investigators in the same field.

The existing literature on this phenomenon tends to fall into two categories: A) Theories of unbounded incident plane waves, concerned primarily with the development of material models which explain the observed amplitude dips and phase shifts; and B) Theories, where the incident waves are bounded, which attempt to describe what happens when a bounded rather than an unbounded beam is involved. In principle, all theories of this type are extensions of the unbounded theories. Their primary goal is to explain a variety of puzzling nonspecular effects, such as the beam shift effect first observed by Schoch.<sup>6</sup>

In section 5 we will review two of the more interesting and successful theories, namely that of Richardson and Becker<sup>13</sup> and that of Pitts<sup>24</sup>, <sup>25</sup> and similar theories.<sup>26-29</sup>

## 4.0 SUMMARY OF RESEARCH RESULTS (PHASE I)

In the following section, we describe experimental results on a set of controlled and uncontrolled samples. General statements regarding the qualitative features of the data are made before discussing the prospects of direct comparison of these results with existing theory.

### 4.1 Samples

Existing literature on the subject of the critical angle scattering phenomenon has focused largely on a theoretical explanation with only modest experimental support. That is not to say that published experiments do not agree with published theories; rather the number and types of materials examined does not seem to constitute a very serious test of these theories. Accordingly, we undertook a preliminary survey of the experimental properties of a wider class of materials. We have examined:

- 1) Naturally occurring minerals and rocks (uncontrolled) including single crystals of quartz, fluorite, and calcite
- 2) Single crystals (controlled) of silicon and saphire
- 3) Alloys (controlled and uncontrolled) of aluminum, iron, titanium, copper, and brass
- 4) Composites such as an aluminum carbon fiber composite
- 5) Glasses such as fused silica and obsidian
- 6) "Ceramics" such as alumina, tungsten carbide, and tungsten powder composites

Only the alloys, ceramics, and composites are of direct interest to the NDT community; however, our understanding of the theory can be improved by examining the response of simple single crystals rather than complex polycrystals such as alloys. We included rocks and minerals in this survey in order to discover possible anomalous behavior due to the complex structure and chemical composition often exhibited by these naturally occurring materials.

#### 4.2 Temperature Control

All experiments were performed at a temperature of 25°C. This was essential for accurate, reproducible measurements as illustrated in Figure 6 where the critical angle for a titanium sample is plotted vs. temperature for T = 5 to 25° C.

Because the apparatus may exhibit some distortions with a change of temperature and because the surface and bulk velocities (of the sample and the water bath) are functions of temperature, there are considerable changes in  $\theta$  with changes in T. In Figure 6 for Ti, we find  $\Delta\theta/\Delta T \approx (.1^\circ)/(^{\circ}\text{C})$ . The heat bath employed was sufficiently stable to allow measurements of  $\theta$  to about  $\pm .025^\circ$  or better as shown in Figure 7.

#### 4.3 Experimental Procedure

Samples with existing flat but rough surfaces were prepared by grinding these surfaces with #100 and #600 carborundum in that order. The sample was then placed in the gimbaled sample holder and the

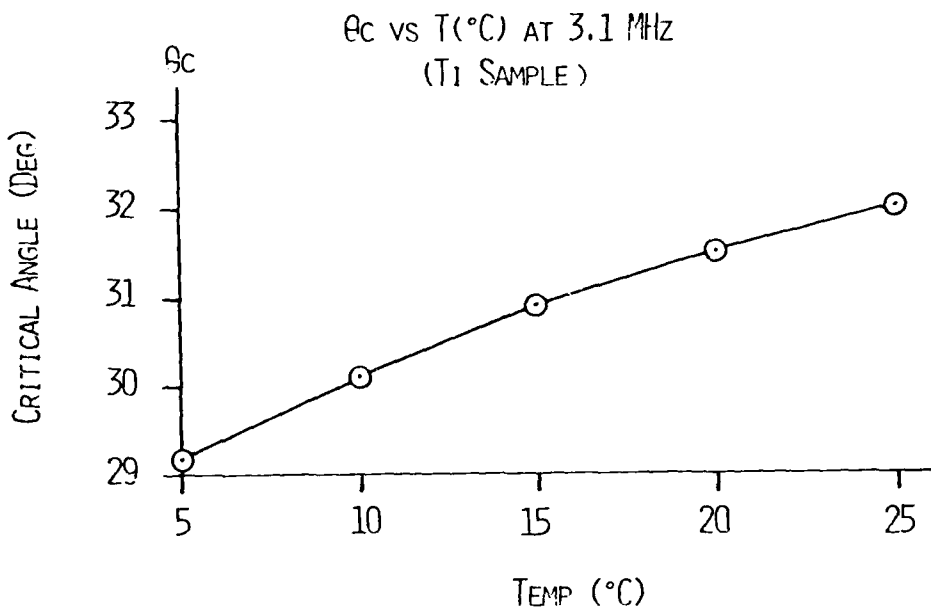


FIGURE 6. TEMPERATURE EFFECTS. A SAMPLE OF TITANIUM WAS EXAMINED AT A SERIES OF TEMPERATURES RANGING FROM 5 TO 25°C. STRAINS IN THE APPARATUS AND CHANGES IN VELOCITY IN BOTH THE WATER BATH AND THE SPECIMEN CONTRIBUTE TO CHANGES IN THE CRITICAL ANGLE  $\theta_c$ . IT IS CLEAR THAT TEMPERATURE VARIATIONS ARE IMPORTANT IN SUCH MEASUREMENTS SINCE WE OBSERVE A CHANGE OF APPROXIMATELY 1° IN  $\theta_c$  FOR 5° C (BETWEEN 10 - 15° C) CHANGE IN TEMPERATURE.

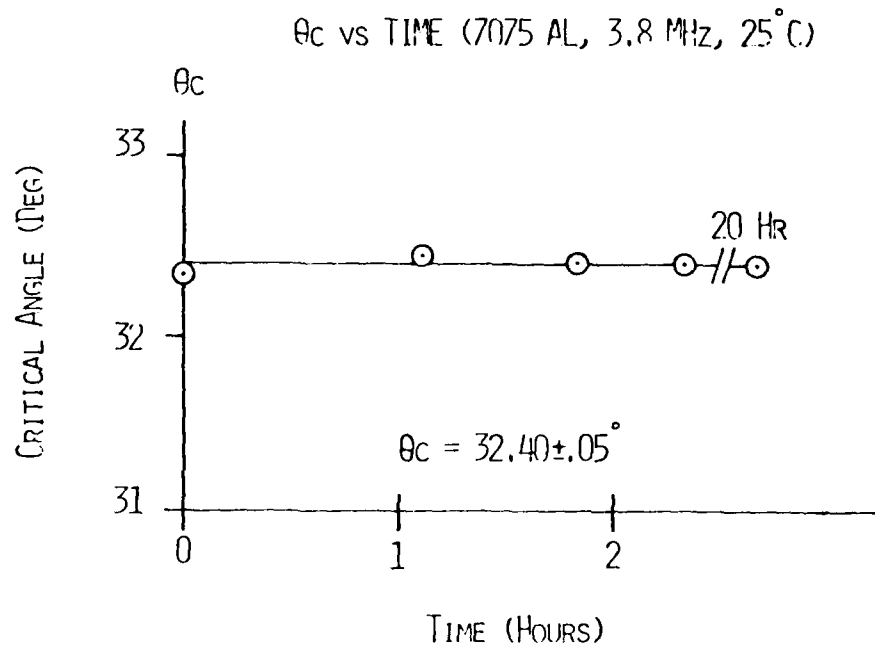


FIGURE 7. REPRODUCIBILITY OF MEASUREMENTS. AN ALUMINUM SAMPLE WAS MAINTAINED AT 25° C AND MEASUREMENTS OF  $\theta_c$  WERE MADE OVER A PERIOD OF HOURS. A NUMBER OF MEASUREMENTS WERE ALSO MADE AFTER REPEATEDLY REPLACING AND REMOVING THE SAMPLE. THESE MEASUREMENTS (NOT SHOWN) HAD ESSENTIALLY THE SAME ERROR AS THE SAMPLE THAT WAS NOT REMOVED DURING THE SERIES OF MEASUREMENTS.

goniometer placed in a small water tank. The water (clean tap water) is circulated in a temperature control reservoir, and all measurements are made at 25°C. When fresh water is initially placed in the reservoir, circulation for several hours is required to eliminate dissolved gasses that would result in bubble formation on the transducers and the sample surface.

When the sample is in place and the system temperature has equilibrated, the goniometer is calibrated by setting up on a known angle ( $\theta = 30^\circ$ ) which is the initial state assumed by the computer-control software.

After the appropriate electronic settings are made, the gimbaled sample holder is properly oriented. This is done by instructing the goniometer from the computer keyboard to move to an incident angle  $\theta = 45^\circ$ . This angle is usually far from any critical angle for most materials (see Table I). If it does happen to fall on a critical angle, one can set up at any other angle provided  $\theta \neq \theta_{cr}$  where  $\theta_{cr}$  is the surface wave critical angle.

The gimbaled sample holder is then roughly leveled by eye. Next, fine adjustments are made on the gimbaled sample holder until the reflected signal amplitude  $R(\theta)$  is a local maximum at the chosen angle. When this occurs, the sample is assumed to be properly oriented in space and a measurement can then be made.

A reconnaissance run on the sample is then made to locate the critical angle. Data is plotted on a CRT and examined visually to locate the angle. More appropriate initial, final and angle

increments can then be keyed in if necessary and a final run made.

The entire procedure, given a properly prepared sample, takes less than five minutes per sample. Data stored on disc cartridges can be called up for analysis or examination at a later date.

#### 4.4 Qualitative Features of Experimental Data

Before discussing what may be called "anomalous" experimental results, let us describe the general qualitative features of those sample measurements that are more or less similar to theoretical predictions. In Figure 8, we illustrate schematically a "typical" curve for  $R(\theta)$  and  $\phi(\theta)$  vs. the incident angle  $\theta$ .

At point A,  $\theta$  is equal to the shear critical angle; that is, the angle  $\theta_s$  at which the shear wave propagates along the water-solid boundary. From Snell's law, this condition reads

$$\frac{\sin \theta_s}{v_w} = \frac{\sin \pi/2}{v_s} = \frac{1}{v_s} \quad (4)$$

$$\theta_s = \sin^{-1} (v_w/v_s) \quad (5)$$

where  $v_w$  is the longitudinal velocity in water and  $v_s$  is the shear wave velocity in the solid.

From A to B, the amplitude  $R(\theta)$  begins to drop and a shift in the phase  $\phi(\theta)$  begins. At point B,  $R(\theta)$  approaches a minimum and the rate of change of the phase is maximal. Finally, at point C there is a local maximum in  $R(\theta)$  before  $R(\theta)$  settles down to a more or less

constant value.

These results are similar but not identical to theoretical predictions for unbounded beams,<sup>13, 15, 24</sup> It is well to keep in mind the fact that we are examining a very small portion of a nonuniform reflected beam that results from a special kind of bounded beam (a focused beam). Figure 9 illustrates the experimental arrangement we employed which involves a focused lens system and a "point" receiver (.1 mm). This point receiver is designed to examine only one "wavevector" out of the range of wavevectors incident on the sample. As such, this experimental arrangement to a certain extent eliminates the problem of examining the beam profile. Only the component that is in the location of the "would be" specular reflection along the axis of the lens is being examined. Trailing waves, which result from the reradiation of the surface wave back into the water, are largely eliminated.

Basically, the point receiver should produce results comparable to an unbounded beam. Therefore, comparisons between our results and the unbounded beam theories appear to be appropriate, at least in a first approximation.

#### 4.5 Results and Anomalies

A rather "typical" experimental curve is illustrated in Figure 10. The specimen was a titanium alloy (6AL-2Cb-1Ta-1Mo), and measurements were performed at 25°C and 3.1 MHz. The general qualitative features described in Figure 8 are seen to be present

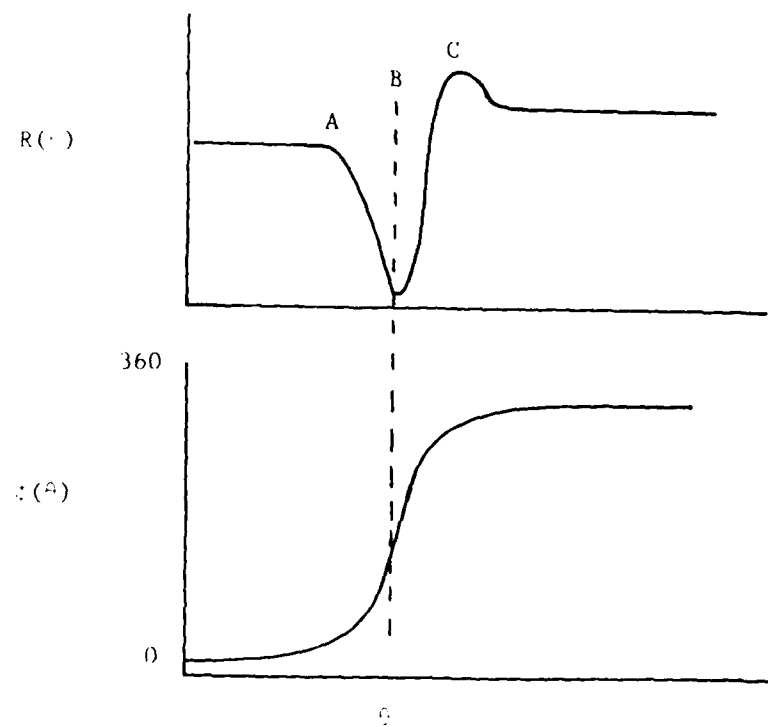


FIGURE 8. SCHEMATIC DIAGRAM OF A TYPICAL EXPERIMENTAL CURVE FOR THE REFLECTED AMPLITUDE  $R(\theta)$  AND PHASE  $\phi(\theta)$  OF THE REFLECTED WAVE.

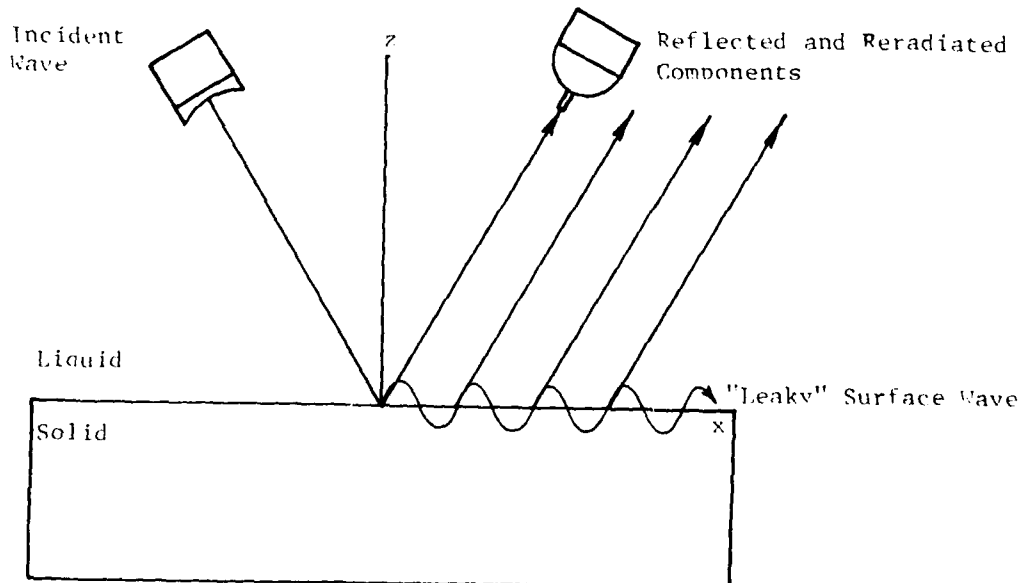


FIGURE 9. EXPERIMENTAL ARRANGEMENT OF THE SOURCE AND RECEIVER.

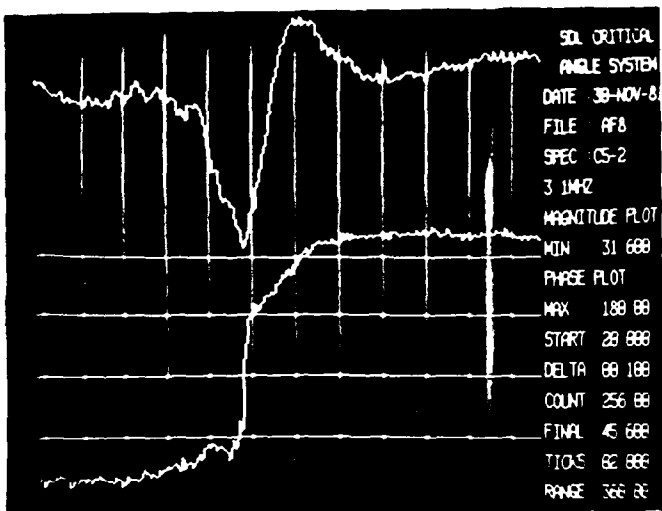


FIGURE 10. EXPERIMENTAL MEASUREMENTS ON A TITANIUM ALLOY AT 3.1 MHZ (25°C) SHOWING THE REFLECTED AMPLITUDE (RELATIVE UNITS)  $R(\%)$  IN THE UPPER CURVE AND THE PHASE  $\phi(^{\circ})$  LOWER CURVE. IN THESE CURVES, THE TIC MARKS ARE  $2^{\circ}$  AND THE RANGE OF THE PHASE DATA IS  $360^{\circ}$ . THE DATA AT THE RIGHT SUPPLIES FURTHER INFORMATION REGARDING THE SPECIMEN.

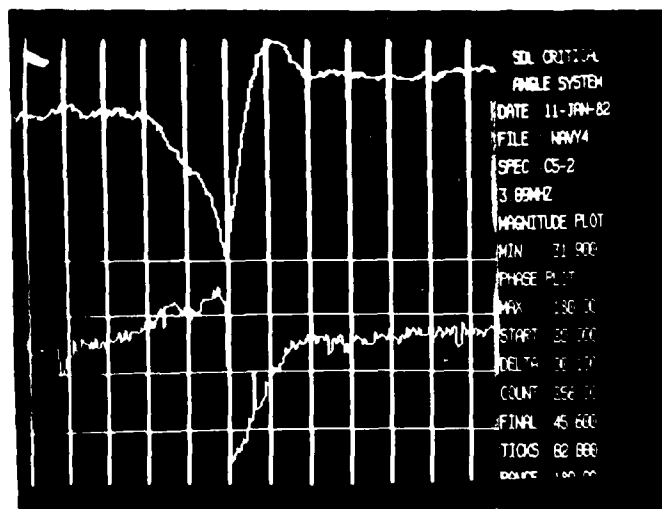


FIGURE 11. SAME SPECIMEN AS SHOWN IN FIGURE 10, BUT WITH A BETTER MINIMUM IN  $R(0)$ . DISTORTIONS IN THE PHASE CURVE  $\phi(^{\circ})$  (BOTTOM CURVE) ARE READILY APPARENT.

in this measured data.

However, a considerable number of "anomalies" are also encountered in making these measurements. When we are careful to locate the frequency of least reflection (FLR) and when we have very carefully oriented the sample (see Experimental Procedure Section 4.3), we often observe a "distorted" phase curve for the same sample (see Figure 11).

In the earlier experiments, we were inclined to attribute these phase curve "distortions" to experimental error since they were evidently very sensitive to set up parameters. However, after we introduced temperature controls and a gimbaled sample holder, it was shown that results were highly reproducible. That is, a sample could be measured, removed, and then remeasured with nearly identical results. Thus, we found that at the same frequency, temperature, sample elevation, and orientation (and direction of examination along the surface) we obtained essentially identical amplitude curves.

Slight changes in the orientation of the normal to the sample surface could result in the appearance of distinct distortions in the phase curves at the minimum. We soon noticed that when these distortions occurred, we invariably had produced the least minimum in the amplitude curves. That meant that we had in fact an even better set up than the original measurement (using standard experimental procedure of setting up on 45° and maximizing the reflected amplitude by adjusting the sample orientation) which had produced an "undistorted" phase curve.

At this point in our experiments, we decided to examine the actual reflected signals at the minimum amplitude location. If this signal contains some unwanted component, it could explain the anomalous phase curves. In Figure 12 we illustrate in schematic form the typical waveforms observed near the minimum of the reflected amplitude.

Signals of this type are invariably seen in numerous samples whenever a distorted phase curve is seen. By slightly changing the sample orientation until the signal amplitude increases, the signal distortions become less obvious to the eye and a "good" phase curve is again obtained. This explains why the sample orientation is so important in observing this effect.

There is clearly a second harmonic contamination present in these signals. We have observed that as the primary reference frequency is increased, the harmonic frequency increases accordingly. Because this second harmonic contamination is of comparable amplitude to the incident wave (at  $\theta_c$ ) at the minimum of  $R(\theta)$ , it was at first thought that this was the cause of the distorted phase curves.

However, the vector volt meter (phase and amplitude measuring system) we are employing was designed to be insensitive to a second harmonic contamination of this magnitude (it is filtered out). Thus, in spite of the very obvious second harmonic contamination, it is not responsible for the observed phase curve distortions.

By band-pass filtering the received signal, it was eventually found that these phase distortions are due to signals at the original

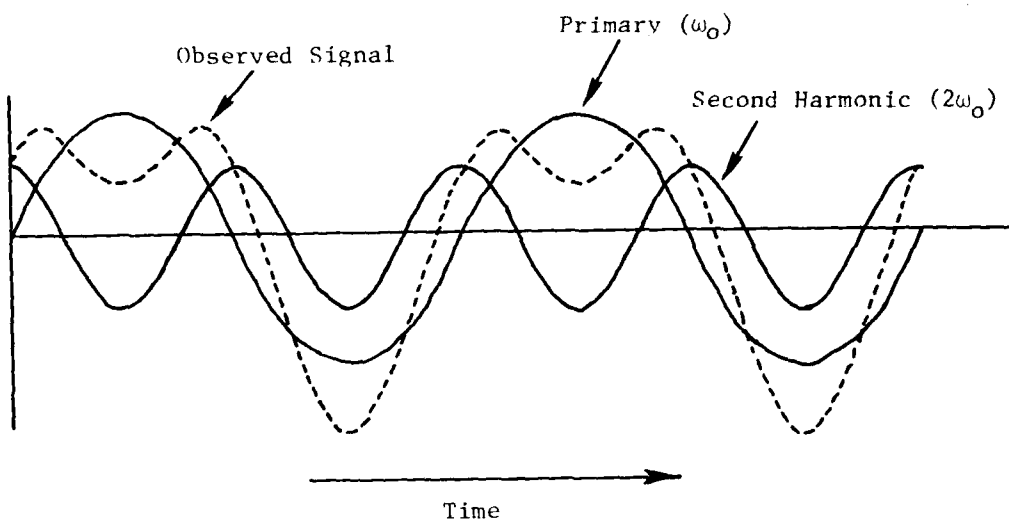


FIGURE 12. SCHEMATIC DIAGRAM SHOWING THE OBSERVED SIGNAL AT THE MINIMUM OF  $R(\theta)$ . THIS SIGNAL APPEARS TO BE THE SUM OF A PRIMARY WAVE OF FREQUENCY  $\omega_0$  AND A SECOND HARMONIC FREQUENCY  $2\omega_0$  AT  $90^\circ$  TO THE PRIMARY. WHENEVER SUCH A SIGNAL WAS OBSERVED, THE PHASE CURVES WERE INVARIABLY DISTORTED. HOWEVER, IT WAS SOON LEARNED THAT THIS SECOND HARMONIC CONTAMINATION WAS NOT RESPONSIBLE FOR THESE DISTORTIONS SINCE THE PHASE METER DID NOT RESPOND TO THIS COMPONENT (SEE TEXT FOR A DISCUSSION).

reference frequency  $\omega_0$ .

We tentatively conclude that this additional component at the reference frequency  $\omega_0$  is the result of some effect due to transmission through the water, a sample dependent effect, or both. We note that nonlinear interactions could be responsible either in the water or the sample or both.<sup>30-34</sup> If this is the case, the signal at the reference frequency  $\omega_0$  would have to interact, say with a second harmonic at  $2\omega_0$ , to yield a signal at  $2\omega_0 - \omega_0 = \omega_0$ . It is very difficult to say at this time just what the mechanism is. Other possibilities still cannot be eliminated. We are certain, however, that these effects are not due to electronic contamination or other peculiarities of our experimental apparatus. These effects are definitely occurring along the sound path and there are indications that it is the sample and not the water path that is introducing this new signal. It also begins to look as if this phase distorting signal only appears when we are at a critical angle.

To see this, we will now discuss the second kind of anomaly that is frequently observed on the same sample. In Figure 11 it may be noted that just to the left of the minimum in  $R(\theta)$  (about  $2 1/2^\circ$  or 1/4 tick mark on the photo), there is a slight indication of a second minimum since the average slope is smaller in this region. We discover in fact that by rotating the specimen  $90^\circ$  (smaller angles also work) in the plane of its surface about its normal vector we obtain the measurements shown in Figure 13(a).

In this figure there are clearly two dips and two associated

"distorted" phase shifts. Again it should be stressed that measurements of this sort are repeatable, nor are these multiple dips unusual. We see indications on many samples of a second dip. Two of the most dramatic results being those found in  $\text{CaF}_2$  and a 4340 steel (see Figures 13(b) and (c)). It is clear from Figure 13 that the mechanism causing the phase distortions (whatever its exact nature) is present at each dip but does not seem to be present elsewhere. This strongly implies that the effect (phase distortions) is sample dependent.

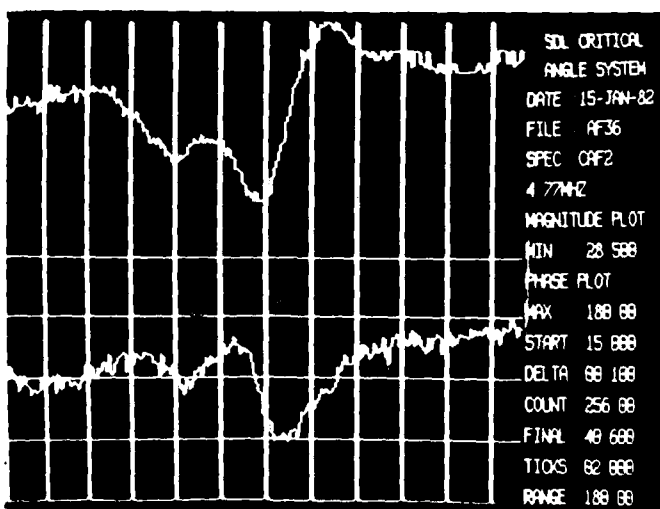
Apart from these observations regarding phase distortions, the very existence of multiple dips is a surprising and completely unexpected phenomenon. None of the existing theories predict such an effect. A preliminary interpretation, which is by no means the only possible interpretation, is that a surface wave is being generated at each of these amplitude dips. If this were the case, we must definitely reexamine the theoretical foundations since conventional theories with conventional boundary conditions predict only one surface wave along a liquid-solid interface (isotropic solid).<sup>35</sup>

In Table I, we list the results for  $\theta_c$  at the frequency of least reflection on several different types of materials.

FIGURE 13. MATERIALS SHOWING MULTIPLE AMPLITUDE DIPS. IN (c) A TITANIUM SPECIMEN SHOWING TWO DIPS AND TWO DISTORTED PHASE SHEETS IS REPRODUCED. THE TWO DIPS ARE SEPARATED BY ROUGHLY 3°. SIMILARLY, IN (d) A CALCIUM FLUORIDE CRYSTAL SHOWS TWO AMPLITUDE DIPS SEPARATED BY ABOUT 4°. FINALLY, IN (e) AND (f) WE ILLUSTRATE TWO MEASUREMENTS (ONE AUTOMATED AND THE OTHER A HAND MEASURED CURVE) ON A 4340 STEEL SPECIMEN. IN THE HAND MEASURED CURVE, THERE ARE CLEARLY TWO DIPS. INDICATIONS OF A THIRD AMPLITUDE DIP APPEAR IN THE AUTOMATED MEASUREMENT.



13(c) TITANIUM SPECIMEN (3.4 MHZ)



13(d) CALCIUM FLUORIDE (4.7 MHZ)

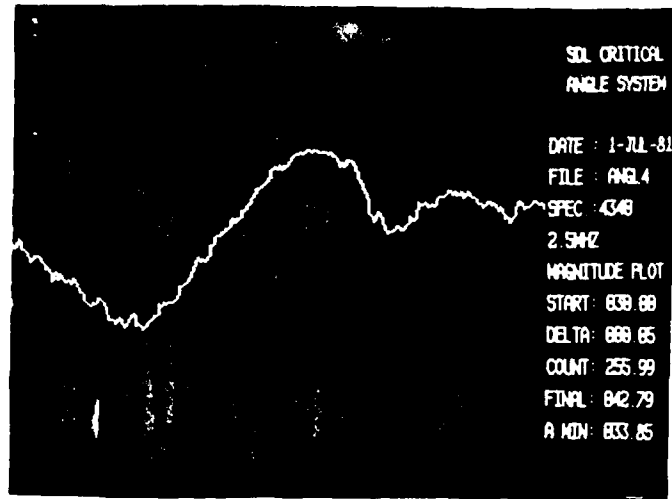


FIG. 1360. MAGNITUDE OF REFLECTED WAVE.

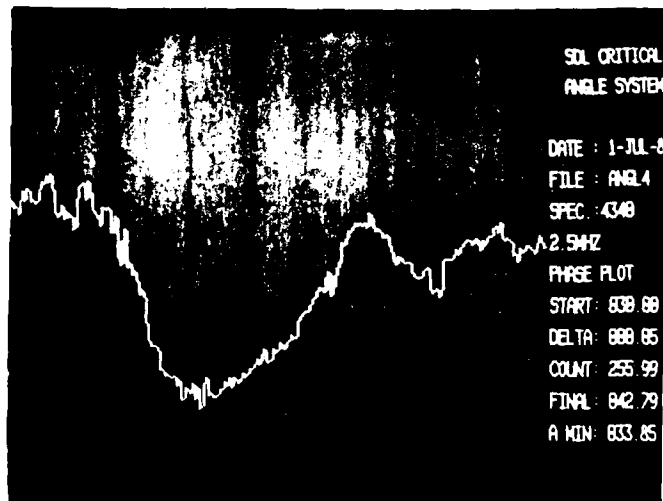


FIG. 1360. PHASE OF REFLECTED WAVE.

FIGURE 1360. PLOTS OF MAGNITUDE AND PHASE (DIPS) VS.  $\theta$  FOR  
 FROM 30° TO 43°. THE SPECIMEN CA 4340 STEEL.  
 SPECIFIC SHOWN THREE AMPLITUDE "DIPS" AND THREE  
 ASSOCIATED PHASE SHIFTS AT THREE DISTINCT ANGLES.  
 THE MOST PRONOUNCED DIP OCCURS AT 33.9°.

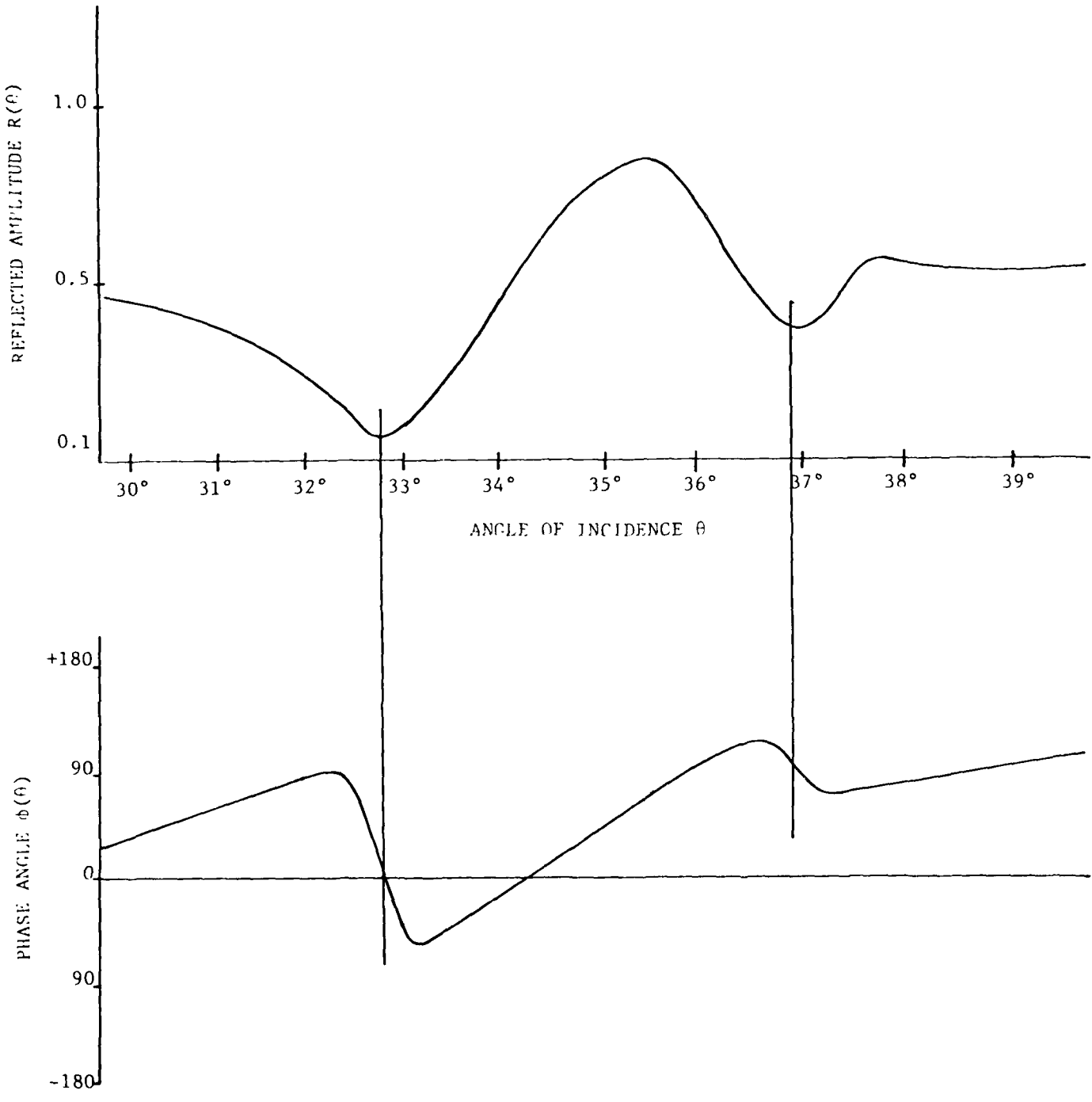


FIGURE 13(d). A 4340 STEEL SPECIMEN (HAND MEASUREMENT)

TABLE I: PRINCIPAL CRITICAL ANGLE  $\theta_c$  FOR VARIOUS MATERIALS AT THE FREQUENCY OF LEAST REFLECT FLR

Metals and Alloys

	$\theta_c$ (°)	FLR (MHz)
Copper	47.5	4.46
Brass	50.7	2.14
Aluminum(7075)	33.5	4.29
Titanium	31.6	3.10
4340 Steel	33.8	2.50
Woods Metal	----	---- (no $\theta_c$ 15-55°)

"Ceramics"

Tungsten Carbide	----	---- (no $\theta_c$ 15-55°)
Tungsten Powder Composite	37.8	4.9
Alumina(Coors)	17.8	4.9

Polymers

Rubber	----	---- (no $\theta_c$ 15-55°)
Polystyrene	----	----

Glasses

Obsidian	26.9	2.62
Silica	26.5	2.55

Complex Silicates

	$\theta_c$ (°)	FLR (MHz)
Granite(fine grained)	26.2	4.00
"Tiger Eye"	25.2	4.00
Epidote	25.0	5.00

Single Crystals

Silicon(Si)	21.1	4.45
Saphire(Al <sub>2</sub> O <sub>3</sub> )	15.6	3.79
Fluorite(CaF <sub>2</sub> )	28.5	4.77
Quartz(SiO <sub>2</sub> )	28.6	3.74

#### 4.6 Frequency of Least Reflection (FLR)

An examination of the data of Table I shows that the measured frequencies of least reflection are typically less than 5 MHz for a wide range of material types.

This observation was somewhat surprising since other authors report FLR's typically above 10 MHz. Richardson has also indicated (private communication) that in experiments performed by Becker and Richardson, the minimum at FLR did not appear to be as deep as we generally find. We have not yet determined the cause of these differences but since our electronics responds well in the range where measurements were made, we are confident that these FLR's are correct. It is possible that some aspect of our experimental apparatus, such as the focused lens, is responsible for these differences. However, it does not seem likely that a function which undergoes a minimum ( $R(\theta)$ ) and which depends on material properties will be effected by a different measuring procedure. The minimum will still occur at a frequency  $\omega(FLR)$  which should be essentially independent of the apparatus used to observe it.

For these reasons, our experimentally determined FLR's seem to be at odds with those found by other investigators although we have not examined the same samples as these investigators.

## 5.0 PROSPECTS FOR COMPARISON OF EXPERIMENTS WITH EXISTING THEORIES

A number of authors working independently have arrived at rather similar theoretical descriptions for the critical angle phenomenon in spite of what at first appears to be different assumptions.

We will discuss here the work of Richardson<sup>13</sup> and that of Pitts<sup>24</sup> as representative of the available theories. Various qualitative predictions made by these models will be discussed and characterized. Comparison between these predictions and our experimental results will be made. Questions will then be raised regarding possible modifications of these theories.

### 5.1 The Richardson Model

It has been known experimentally for some time that at a critical angle both an amplitude dip and a phase shift occur in a reflected acoustic (or elastic) wave incident on a boundary between two solids (or a solid-liquid boundary).<sup>6-8</sup> The mechanism for this behavior is the conversion of the incident longitudinal or pressure wave into a surface or Rayleigh-type wave that propagates along the boundary and extends roughly one wavelength into the media on either side of the boundary. This conversion of incident wave energy to surface wave energy and the subsequent reradiation back into the water accounts for the dip in the amplitude of the reflected wave.

Until recently, however, the theory for this behavior was unsatisfactory. Whereas surface wave solutions have long been known to exist in classical "hookean" materials,<sup>35</sup> the mechanism for exciting these waves was not well understood until attenuation was added to the analyses. The Richardson linear visco-elastic wave model among others has updated the classical Hooke's law theory by including the effects of attenuation via the addition of "viscous" terms in the stress-strain relation. It has been found that these viscous terms indirectly determine the coupling between an incident wave and the respondent surface wave. Without such terms, very little if any surface wave energy will result at the boundary between two media.

Richardson's linear visco-elastic model in a one-dimensional approximation may be described by the stress-strain relation

$$\sigma = K_1 \varepsilon + \frac{K_2}{\omega} \dot{\varepsilon} \quad (6)$$

where higher order terms involving  $\ddot{\varepsilon}$  etc. are assumed to be unimportant, and where the "viscosity" coefficient  $n = K_2/\omega$  is frequency dependent. This is another way of saying that the "response time"  $\tau$  is distributed as  $1/\omega$

$$\tau = \frac{K_2}{K_1 \omega} . \quad (7)$$

Using this simple model, it is easily shown that the stress-strain

ellipse is frequency independent since we find for  $\epsilon = \sin \omega t$

$$\epsilon^2 + \left( \frac{\sigma - K_1 \epsilon}{K_2} \right)^2 = 1 . \quad (8)$$

Frequency independence of the  $\sigma - \epsilon$  ellipse was shown by Knopoff<sup>36</sup> to be an observed property of many materials over a very wide range of acoustic frequencies. Richardson and Becker<sup>11</sup> have shown experimentally that this frequency independent behavior also holds for metals and other similar materials in the MHz range of frequencies.

By generalizing Equation (4) to a tensor equation in three dimensions

$$\sigma_{ij} = c_{ij}^{kl} \epsilon_{kl} + \frac{D_{ij}^{kl}}{\omega} \epsilon_{kl,t} , \quad (9)$$

Richardson was able to derive the modified elastic wave equations describing the propagation of P and S waves in isotropic, homogeneous media. From these equations, he was then able to solve the particular problem of the reflection of an incident wave from the boundary between two dissimilar media. In particular, he found the reflection coefficient at a liquid-solid boundary.<sup>13</sup> Working independently, Merkulova arrived at the same result.<sup>15</sup> The essence of the theory resides in the equation for the reflection coefficient found by these authors

$$R = \frac{\cos^2 2\gamma_{22} + (c_{22}/c_{12})^2 \sin 2\gamma_{12} \sin 2\gamma_{22} + \rho_1 c_{11} \sin \gamma_{12} / \rho_2 c_{12} \sin \gamma_{11}}{\cos^2 2\gamma_{22} + (c_{22}/c_{12})^2 \sin 2\gamma_{12} \sin 2\gamma_{22} - \rho_1 c_{11} \sin \gamma_{12} / \rho_2 c_{12} \sin \gamma_{11}} , \quad (10)$$

where  $c_{12}$  = velocity of longitudinal waves in the solid,  
 $c_{22}$  = velocity of shear waves in the solid,  
 $c_{11}$  = velocity of longitudinal waves in the liquid,  
 $\theta = \gamma_{11}$  = angle of incidence of the longitudinal wave in the liquid,  
 $\gamma_{12}$  = angle of refracted longitudinal wave in the solid,  
 $\gamma_{22}$  = angle of refracted shear wave in the solid,  
 $\rho_1$  = density of liquid  
 $\rho_2$  = density of solid.

Angles are measured in the counterclockwise direction from the x-axis  
 (plane of the interface). The velocities are the complex quantities

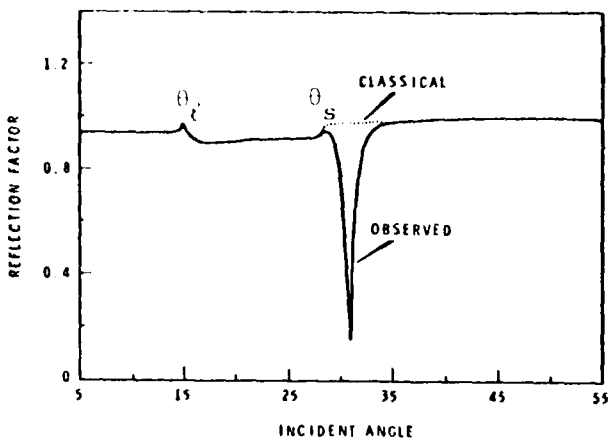
$$c = v(1 + iv\alpha/\omega), \quad (11)$$

$v$  = normal velocity,  
 $\alpha$  = attenuation,  
 $\omega$  = radian frequency.

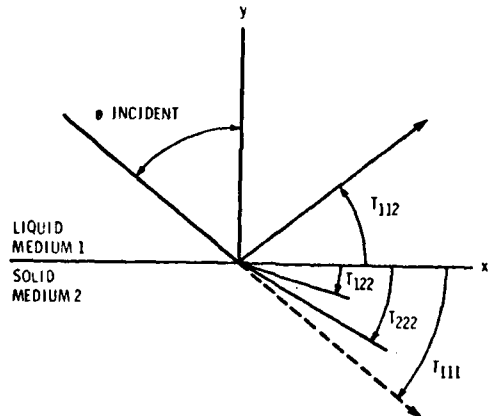
The refracted angles are found by the generalized Snell's law,

$$\frac{\cos\gamma_{ij}}{c_{ij}} = h. \quad (12)$$

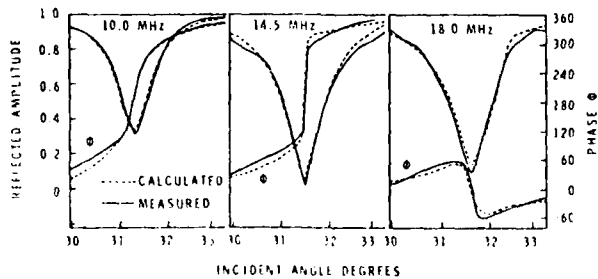
These equations have been specialized to a two layered  
 liquid-solid medium although the theory holds for solid-solid  
 interfaces as well. This model is said to predict observed behavior  
 for unbounded beams with good accuracy. Both the dip in amplitude



REFLECTED AMPLITUDE VERSUS ANGLE OF INCIDENCE FOR A WATER/STAINLESS STEEL INTERFACE. THE OBSERVED REFLECTION FACTOR (SOLID LINE) DIFFERS FROM THAT CALCULATED BY NONATTENUATION WAVE MODELS (DASHED LINE) IN THE AREA OF THE RAYLEIGH CRITICAL ANGLE.



COORDINATE SYSTEM  
FOR RICHARDSON'S CALCULATION



CALCULATED AND MEASURED PHASE AND AMPLITUDE OF REFLECTED WAVES AT A WATER-304 STAINLESS-STEEL INTERFACE FOR FREQUENCIES OF 10.0, 14.5, AND 18.0 MHz FOR RICHARDSON'S MODEL.

and the phase change are predicted quantitatively as well as qualitatively.

In addition to describing the behavior of the reflected wave at the critical angle, the theory indicates that there exists a frequency at which there is zero reflection at the critical angle called the frequency of least reflection (FLR). This point is said to be highly dependent upon grain size, and appears to present a method for its measurement.

The theory developed by Richardson is nearly complete with respect to the steady state solution. In the course of the experimental verification, however, some interesting transient effects were observed.<sup>12</sup> It was noted that the phase response near the critical angle involved a time lag. That is, it took a finite amount of time after initiation of the ultrasonic burst before the phase of the reflected wave changed from the classically predicted value to that obtained with the Richardson theory. Thus, it appears that extension of the theory to include transient effects might be profitable.

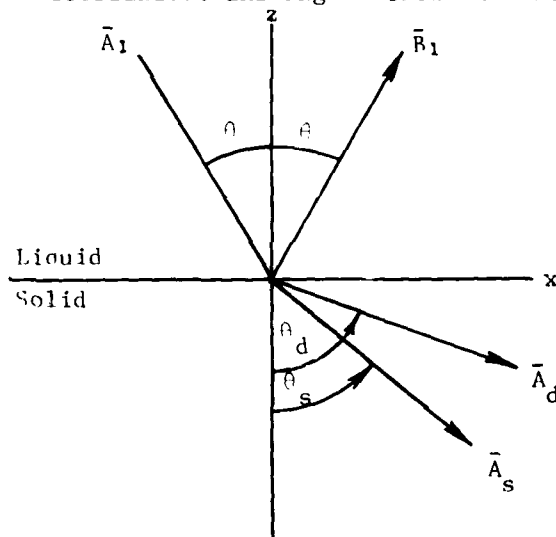
### 5.2 The Model of Pitts

Whereas Richardson has provided a particular model based on a fundamental stress-strain relation including attenuation, Pitts at first appears to take a different and more conventional view by introducing attenuation directly in the wave numbers. The end results of these two approaches are nevertheless rather similar and may ultimately involve identical physical models in some cases. We will review

rather closely the derivation given by Pitts in his 1976 thesis and discuss the approach as we proceed.

Pitts remarks that his derivation follows the standard approach given in most textbooks although his results differ slightly from those of Brekhovskikh<sup>7</sup> for example. In what follows, we will employ a set of symbols that are different than those employed by Richardson. Richardson's formulation does not appear to use "conventional" notation. For example, he employs complex velocities whereas Pitts and others employ complex wavenumbers. These differences may make it difficult to compare the results of these authors, but such differences alone do not lead to formally different answers.

Pitts employs the coordinates and angles shown in the figure below for plane waves



where  $\bar{A}_1$  is the incident sound wave and  $\bar{B}_1$ ,  $\bar{A}_s$ , and  $\bar{A}_d$  are the respondent waves ( $s=\text{shear}$ ,  $d=\text{longitudinal in solid}$ ). The law of reflection is assumed to hold, and the propagation directions of the sound waves are assumed to be given by Snell's law

$$\frac{\sin \theta}{V} = \frac{\sin \theta_d}{V_d} = \frac{\sin \theta_s}{V_s} . \quad (13)$$

Here,  $V$  is the longitudinal wave velocity in water,  $V_d$  is the longitudinal wave velocity in the solid, and  $V_s$  is the shear wave velocity.

Although attenuation is not explicitly introduced at this stage, these velocities and angles should be assumed to be generally complex to account for the attenuation.

Pitts then writes down the particle displacement vectors

$$\bar{U} = \bar{A} e^{i\bar{k} \cdot \bar{r}} e^{-i\omega t} \quad (14)$$

for the two media.

For medium 1 (the liquid):

$$\begin{aligned} \bar{U}^1 &= \bar{A}_1 \exp[ik(x\sin\theta + z\cos\theta) - i\omega t] \\ &+ \bar{B}_1 \exp[ik(x\sin\theta - z\cos\theta) - i\omega t] \end{aligned} \quad (15)$$

For medium 2 (the solid):

$$\begin{aligned} \bar{U}^2 &= \bar{A}_d \exp[ik_d(x\sin\theta_d + z\cos\theta_d) - i\omega t] \\ &+ \bar{B}_d \exp[ik_d(x\sin\theta_d - z\cos\theta_d) - i\omega t] \\ &+ \bar{A}_s \exp[ik_s(x\sin\theta_s + z\cos\theta_s) - i\omega t] \\ &+ \bar{B}_s \exp[ik_s(x\sin\theta_s - z\cos\theta_s) - i\omega t] \end{aligned} \quad (16)$$

The sound wave amplitudes are:

$$\begin{aligned} \bar{A}_1 &= A_1[\cos\theta\hat{k} + \sin\theta\hat{i}] \\ \bar{B}_1 &= B_1[-\cos\theta\hat{k} + \sin\theta\hat{i}] \\ \bar{A}_d &= A_d[\cos\theta_d\hat{k} + \sin\theta_d\hat{i}] \\ \bar{B}_d &= B_d[-\cos\theta_d\hat{k} + \sin\theta_d\hat{i}] \\ \bar{A}_s &= A_s[\sin\theta_s\hat{k} - \cos\theta_s\hat{i}] \\ \bar{B}_s &= B_s[\sin\theta_s\hat{k} + \cos\theta_s\hat{i}] \end{aligned} \quad (17)$$

where the unit direction vectors  $\hat{x} = \hat{i}$  and  $\hat{z} = \hat{k}$ . The symbol  $\hat{k}$  should not be confused with a wavevector  $\hat{k}$  and  $\hat{i}$  should not be confused with  $i = \sqrt{-1}$ .

The following conventional boundary conditions on the stresses and particle velocities are then applied to these solutions.

- A) The normal component of the particle displacement ( $\bar{U} \cdot \hat{k}$ ) is continuous across the boundary
- B) The normal component of stress is continuous across the boundary
- C) The shear stress is zero at the boundary

After considerable manipulation (not included in Pitts' thesis), he finds the following reflection coefficient for the unbounded plane wave

$$R_{LS}(k_x) = N/D \quad (18)$$

where  $k_x$  is the x-component wavenumber of the incident wave and where

$$\begin{aligned} N &= (k_s^2 - 2k_x^2)^2 + 4k_x^2 K_s K_d - \rho k_s^4 K_d / K \\ D &= (k_s^2 - 2k_x^2)^2 + 4k_x^2 K_s K_d + \rho k_s^4 K_d / K \end{aligned} \quad (19)$$

and

$$\begin{aligned} \rho &= \rho_{\text{liquid}} / \rho_{\text{solid}} \\ k &= (\omega/v)(1 + iA/2\pi) \\ k_s &= (\omega/v_s)(1 + iA_s/2\pi) \\ k_d &= (\omega/v_d)(1 + iA_d/2\pi) \\ K &= (k^2 - k_x^2)^{1/2} \\ K_d &= (k_d^2 - k_x^2)^{1/2} \\ K_s &= (k_s^2 - k_x^2)^{1/2} \end{aligned} \quad (20)$$

Note that the loss parameters  $A$ ,  $A_d$ ,  $A_s$  appear in the wave-numbers  $k$ ,  $k_d$ ,  $k_s$  rather than in the velocities  $V$ ,  $V_s$ ,  $V_d$ . Therefore,  $v$ ,  $v_s$ ,  $v_d$  are real and  $V$ ,  $V_s$ ,  $V_d$  are complex.

The function  $R_{LS}(k_x)$  depends both on the incident angle  $\theta$  and the frequency. The frequency dependence enters because  $A$ ,  $A_s$ ,  $A_d$  are generally frequency dependent.

### 5.3 Comparison of Pitts' and Richardson's Models

Although the symbols employed in Pitts formulation of  $R(k_x)$  (Equation 18) are different from those employed by Richardson (Equation 10), these expressions lead to very similar results and are based on rather similar ideas even though they may seem to represent different approaches.

- 1) Both Pitts and Richardson employ the same boundary conditions.
- 2) Although Richardson introduces attenuation at the level of Hooke's law and then seeks solutions to a modified equation of motion, his result should not be formally different from a derivation such as Pitts where solutions which include attenuation are postulated ad-hoc. Both approaches would seem to be satisfactory and could very well lead to identical results. Both approaches are, however, strictly phenomenological.
- 3) A single dip in the amplitude and an associated phase shift are predicted by both models at the critical angle. Both models predict that the phase shift is insensitive to changes in shear wave attenuation whereas the reflection factor ( $R(k_x)$ ) is predicted to be very sensitive to the choice of  $A_s$ .
- 4) Both models predict the phenomenon known as the frequency of least reflection (FLR).

To summarize, we can say that the Richardson model<sup>13</sup> which

produces results identical to those of Merkulova<sup>15</sup> also produces results qualitatively very similar to those of Pitts<sup>24, 25</sup> and others<sup>26-29</sup> who have investigated similar models. Although detailed comparisons have yet to be made, there would seem to be little if any essential physical differences between these models in so far as predictions are concerned.

From our experimental results, there are indications that all of these models may have drawbacks. In this context, the differences between one model and a very similar model are less significant than the apparent inability of any model to explain experimental data.

#### 5.4 Theoretical Difficulties

The analysis of Richardson, Pitts, and other authors that have investigated this problem employ conventional boundary conditions i.e.,

- A) Normal component of particle displacement is continuous across the boundary (liquid-solid)
- B) Normal component of stress is continuous across the boundary
- C) The shear stress is zero at the boundary.

It is also tacitly assumed by these authors that one can examine the ideal case (Hooke's law behavior) and by appropriate modifications, such as the addition of attenuation, (either in a modified Hooke's law response or in the wavenumbers) obtain the actual response of a material or boundary. This of course is the traditional phenomenological approach followed in most treatises on the theory of elasticity. However, this traditional approach raises a number of serious questions of a physical nature.

Consider the standard problem of computing the reflection and transmission coefficients from a plane boundary between two infinite elastic media. In particular, consider the case of a liquid-solid interface.

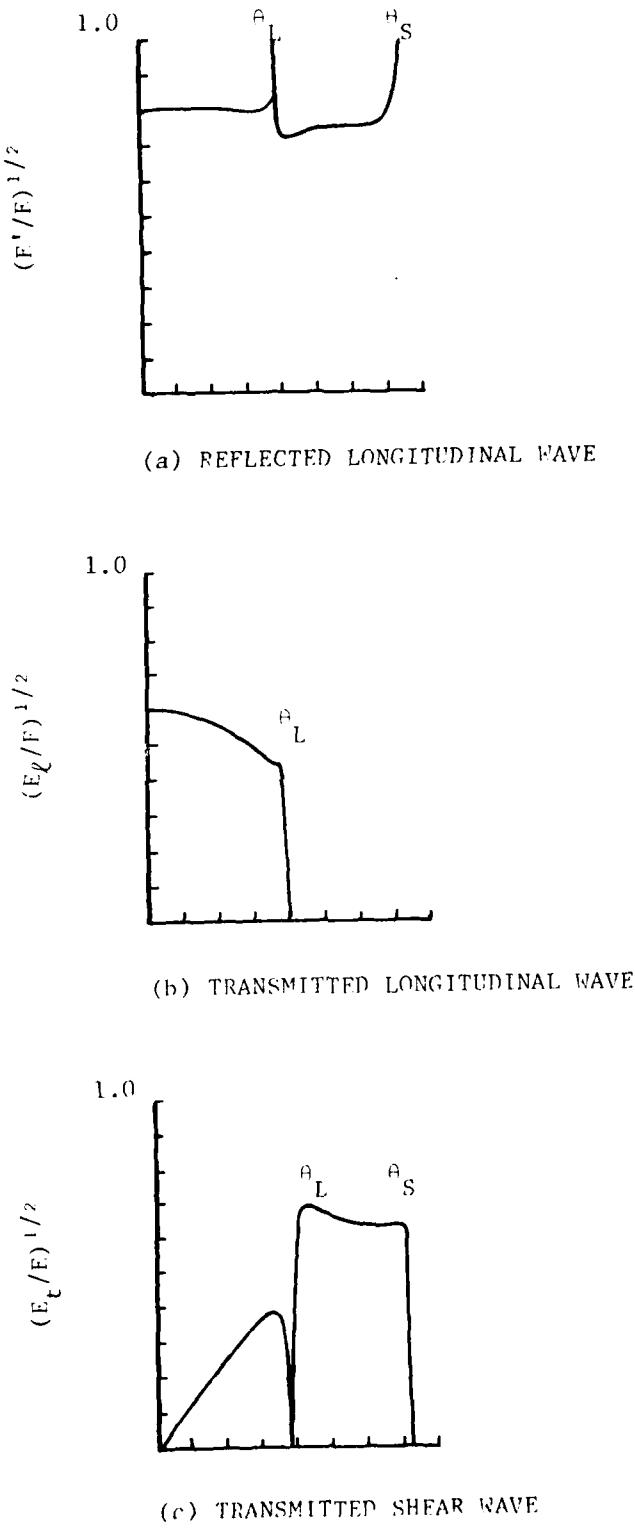
Brekhovskikh,<sup>1</sup> like many other authors in the past, has derived these coefficients for the lossless case and demonstrated that the energy of the elastic waves is conserved. These authors, however, have not apparently gone on to ask if linear momentum is conserved. Consider the reflection and transmission coefficients as derived by Brekhovskikh<sup>1</sup> which is illustrated graphically in his book on page 46 and reproduced in Figure 14.

While it may be satisfying that energy is conserved in this process, a serious question can be raised regarding the correctness of this analysis on the basis of momentum conservation.

Note that both the transmitted shear wave and the transmitted longitudinal wave vanish at the longitudinal critical angle  $\theta_L$ . At this angle, there is 100% reflection of the incident wave ( $E'/E = 1$ ). Similarly, at the shear critical angle  $\theta_s$ , there is 100% reflection of the incident wave  $E'/E = 1$  (see Figure 14). Beyond  $\theta_s$ , of course, we have the additional possibility of the Rayleigh critical angle phenomenon.

Consider then a wave which is 100% reflected from a solid as shown in Figure 15. Let us calculate the change in momentum of this incident sound wave. The x-components of momentum will clearly be unaltered; however, there will be a finite change in the z-component.

FIGURE 14. THE CONVENTIONAL ANALYSIS OF THE REFLECTION AND TRANSMISSION COEFFICIENTS OF A LIQUID-SOLID BOUNDARY UP TO THE SHEAR CRITICAL ANGLE  $\theta_s$ . CURVES TAKEN FROM BREKHOVSKIKH.<sup>1</sup>  $\theta_L$  IS THE LONGITUDINAL CRITICAL ANGLE. IN THE LOSSLESS CASE, ENERGY IS CONSERVED AND  $E = E' + E_t + E_\ell$ . TOTAL REFLECTION OCCURS AT  $\theta_L$  AND  $\theta_s$ .



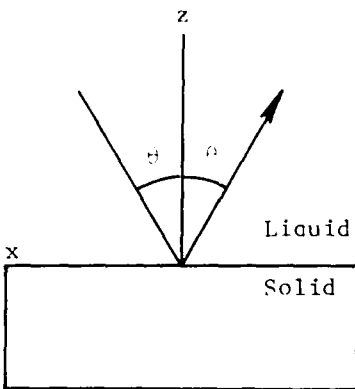


FIGURE 15. A TOTALLY REFLECTED SOUND WAVE. HOW IS THE MOMENTUM TRANSFERRED TO THE SOLID EVEN IF ENERGY IS CONSERVED?

If the wave is essentially unbounded, the group and phase velocities are the same. If  $v$  is the phase velocity in the liquid, the  $z$ -component of momentum of the incident sound wave will be proportional to<sup>30, 37, 38</sup>

$$P_z(i) \propto -\frac{E}{v} \cos\theta . \quad (21)$$

Similarly, the  $z$ -component of the reflected wave will be proportional to

$$P_z(r) \propto +\frac{E}{v} \cos\theta . \quad (22)$$

Thus, the change in the  $z$ -component of the momentum of the totally reflected wave is proportioned to

$$\Delta P_z \propto P_z(r) - P_z(i) \quad (23)$$

or

$$\Delta P_z \propto \frac{2E}{v} \cos\theta .$$

Clearly since  $\theta$  is generally an angle different from  $\pi/2$ , i.e.

$\theta = \theta_s$  or  $\theta_L$ , this quantity is not zero.

By the law of conservation of linear momentum, the change in momentum of the solid must be proportional to  $-\Delta P_z$ . Therefore, momentum must be transferred to the solid from the incident wave.  
This is clearly impossible since no bulk waves exist in the solid at the angles  $\theta = \theta_s$  or  $\theta_L$ .

Thus, the conventional analysis of the lossless case, using conventional boundary conditions, leads to a fundamental error and casts doubt on other similar analyses including the aforementioned analyses of the critical angle phenomenon.

### 5.5 Some Possible Remedies

To illustrate how serious the foregoing paradox is, one need only recall that the same analysis carried out for a totally reflected light beam shows that the momentum transferred upon reflection varies as  $E/c$ .<sup>37</sup> Hence, a sound beam having the same energy density as a light beam carries  $c/v$  times as much momentum. It is acceptable in most optical applications to ignore the small momentum transfers upon reflection (except for very intense beams<sup>39</sup>) but one clearly cannot ignore the relatively large momentum transfers involved in acoustic reflections. How then is the traditional analysis of Brekhovskikh and others to be modified in order to correct such

deficiencies? This question has not as yet been answered, however, we have been able to characterize the problem sufficiently to identify the probable source of these conceptual difficulties.

First, the practice of obtaining approximate solutions by examining a lossless case, as Brekhovskikh does, has a very questionable validity. We note that sound waves are, strictly speaking, impossible unless nonlinearities (interactions) and their inevitable associated losses are present (see Appendix I). This is not a trivial point since it means that even in principle there is no lossless case in acoustics. Such a situation does not even exist in a first approximation. Nor is it possible, strictly speaking, to describe these processes with linear partial differential equations.

Approaches based on these oversimplified phenomenological models (lossless, linear systems) may give reasonable agreement with experience in some situations, but we should not be too surprised if they fail in many others.

A real sound wave carrying energy and momentum incident on a solid, say at a liquid-solid interface, must eventually transfer an amount of energy and momentum to the so called "zero frequency" modes of the solid.<sup>40-43</sup> Such zero frequency modes represent the motion of the solid as a whole. A solid, immersed in a liquid in a state of free-fall and subject to an incident sound pulse (duration  $\tau$ ), would thus begin to translate with a constant average velocity  $V$  (neglecting resistance of the fluid) just after the pulse had left the object. Clearly, there will be an acceleration of the body of

order  $V/t$ . The process of transferring acoustic momentum to the solid is not a linear one since a wave incident at an average frequency of  $\omega_0$  must eventually be converted to these zero frequency modes.

In the language of solid state physics, we can say that the initial phonon spectrum of the solid body has been converted to another spectrum raising the temperature of the solid object. In the process, the zero frequency modes have been excited.

What the foregoing discussion suggests is that the traditional boundary conditions employed in such problems must be altered in order to obtain a consistent theory. The reason for this conclusion is the fact that the interaction at a boundary (liquid-solid) is a local one. At the instant a real sound wave impinges on the boundary, it begins the process of transferring momentum. This can take place in two principal ways on a macroscopic scale:

- A) Via wave-like motions (wave equations)
- B) Diffusion-like motions (damping, viscosity) diffusion equations
- C) Combinations of A) and B).

Wave-like motions, of course, refers to elastic waves, and diffusion-like motions refers to various viscosity terms and leads to transient effects.<sup>12</sup> Now as mentioned, most authors describing the critical angle phenomenon have correctly recognized that the critical angle phenomenon depends in some way on the presence of attenuation. Without attenuation, the phenomenon is certainly inexplicable. These explanations cannot be complete, however, since they employ traditional

boundary conditions. There is no indication that they have resolved the momentum problem for example.

Any narrow region where the solution of a differential equation changes rapidly is referred to in advanced mathematical treatises as a boundary layer. It may well be that the complete solution we are seeking will involve solutions based on Boundary-Layer Theory.<sup>44</sup>

To summarize, we can say that a correct treatment of the Rayleigh critical angle phenomenon will also automatically provide a correct general expression for scattering at all angles; not just the Rayleigh critical angle. In particular, the model will be consistent with energy and momentum conservation in the presence of nonlinearities and losses. Such a model must also explain the phenomenon of multiple amplitude dips and phase shifts.

## 6.0 BRIEF REVIEW OF PHASE II PLANS

The Phase I study has delineated a number of problems with the conventional phenomenological descriptions of the so called Rayleigh critical angle phenomenon. Accordingly, the Phase II program in brief outline will consist of the following elements:

### Task 1: Theoretical Development

Continued Studies in Basic Elasticity Theory

- Damping
- Nonlinearities
- Second Order Effects
- Anisotropy and Discontinuities

Coupling Mechanisms

Momentum Balance (see Figure 16)

Study of Focused Beams

Other Focal Region Effects

- Electromagnetic Properties
- Induced Temperature Gradients
- Applied Stress Effects

### Task 2: Experimental Backup for Task 1

Materials with Double Dips

Monitor Focal Region (see Figure 17)

Experiments in Momentum Balance

Higher Frequency Experiments

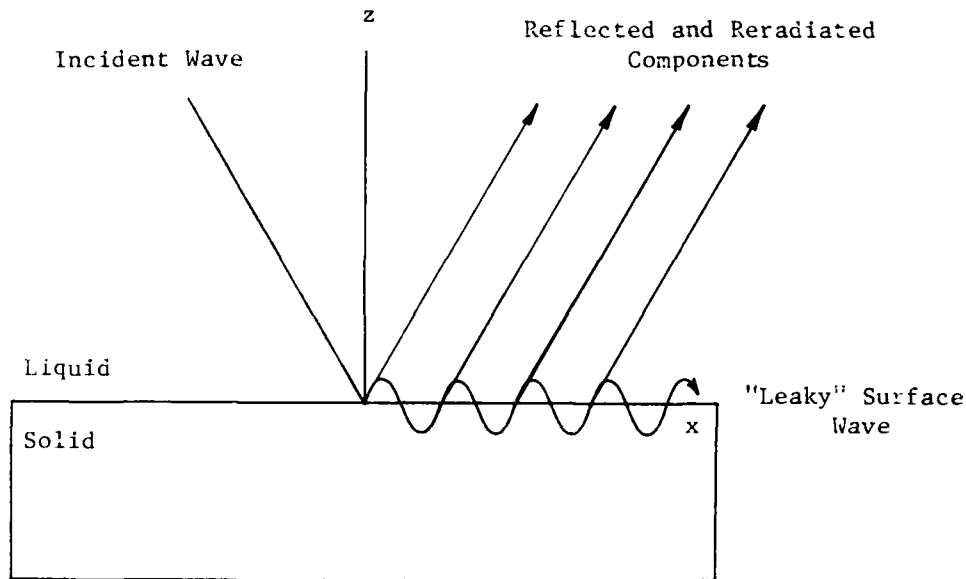


FIGURE 16. THIS FIGURE ILLUSTRATES THE CONVENTIONAL PARTITIONING OF AN INCIDENT WAVE INTO A RESPONDENT "LEAKY" SURFACE WAVE AT THE CRITICAL ANGLE AND REFLECTED AND RERADIATED COMPONENTS. ONE CAN EASILY IMAGINE THAT MOMENTUM IS CONSERVED ALONG X BUT UNLESS THERE IS A BULK WAVE IN THE SOLID, HOW CAN IT BE CONSERVED ALONG Z? IF THERE ARE NO BULK WAVES IN THE SOLID, WE HAVE THE ADDED PROBLEM OF AN UNCOMPENSATED COUPLE (ANGULAR MOMENTUM) DUE TO THE DISPLACEMENT OF THE RERADIATED WAVE.

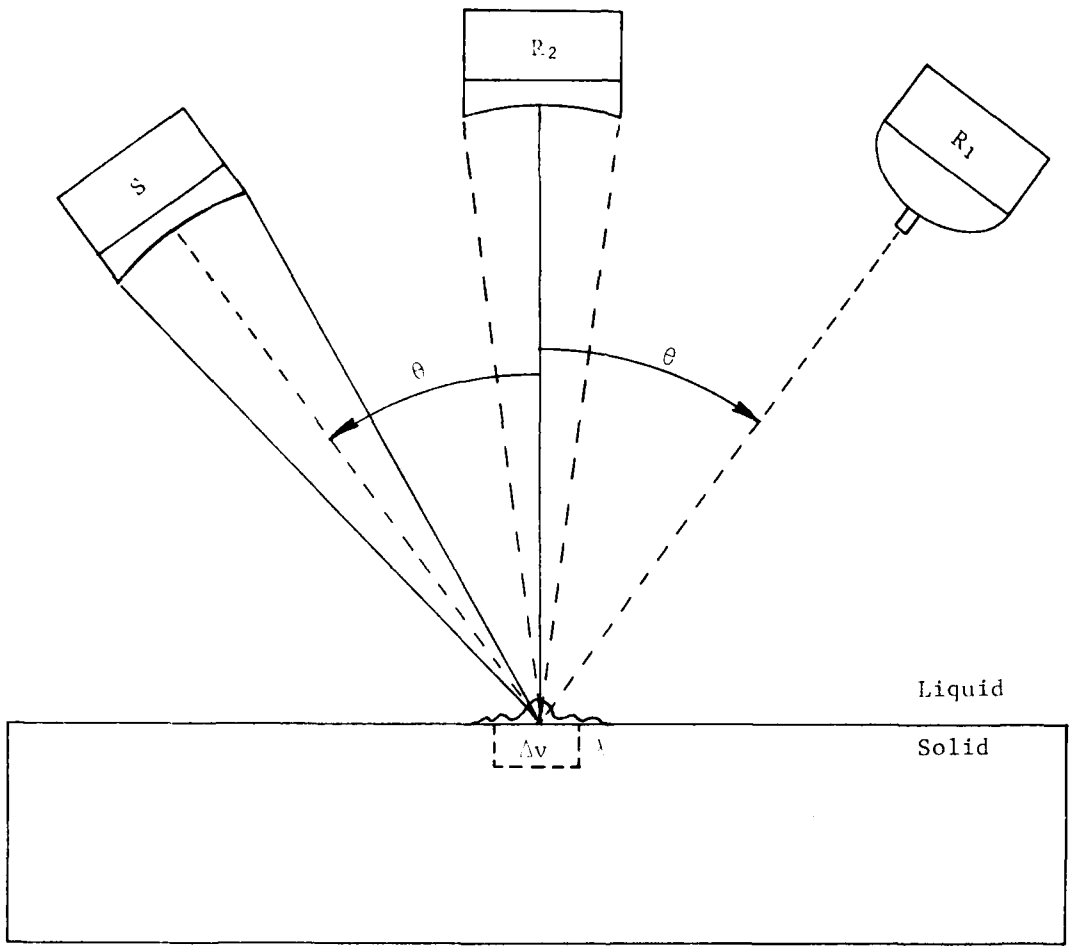


FIGURE 17. THE CRITICAL ANGLE MEASURING SYSTEM CURRENTLY BEING USED EMPLOYS A POINT DETECTOR AT  $R_1$  AND A LENS SOURCE AT  $S$ . IN THE MODIFIED ARRANGEMENT, WE INTEND TO PLACE A FOCUSED DETECTOR (SAME AS  $S$ ) AT  $R_2$ . WE WILL USE THIS TO EXAMINE ANY ISOTROPIC RADIATION COMPONENT FROM THE REGION OF THE "POINT" FOCUS.

## 7.0 SUMMARY AND CONCLUSIONS

The Phase I study of the "Rayleigh" critical angle phenomenon has been completed. An automated, computer controlled goniometer was constructed and perfected. Controlled measurements on a variety of materials, including materials of interest to the NDT community, were carried out and compared with theoretical predictions made by a number of authors.

Experimental results indicate that these theories are only first approximations to reality. We find a number of significant experimental anomalies, such as the appearance of more than one amplitude dip. Certain theoretical questions can also be raised regarding these theories including the question of momentum conservation at the interface. Both the experimental and theoretical observations suggest that we are not yet in possession of a complete theory.

Phase II plans are designed to investigate both experimentally and theoretically these questions so that our goal of a better theoretical understanding of this phenomenon can be achieved. Given this improved understanding, practical quantitative NDT techniques based on the "Rayleigh" critical angle phenomenon will become available.

#### ACKNOWLEDGMENTS

The authors thank R. L. Silta for design and construction of experimental apparatus, and T. J. Davis for aid in understanding harmonic distortions. We would also like to thank Y. M. Pipkin for editing, typing, and assembling this report.

## 8.0 REFERENCES

1. L. M. Brekhovskikh, Waves in Layered Media, Academic Press, New York (1980).
2. J. D. Achenbach, Wave Propagation in Elastic Solids, North-Holland Publishing, New York (1973).
3. B. A. Auld, Acoustic Fields and Waves in Solids, Vol. I & II, John Wiley, New York (1973).
4. D. H. Towne, Wave Phenomena, Addison Wesley, Reading, MA (1967).
5. M. Newlands, J. Acoust. Soc. Am., 26, 434-448 (1954).
6. A. Schoch, Acustica 2, 18 (1952).
7. Brekhovskikh (1960).
8. F. R. Rollins Jr., "Ultrasonic Reflectivity at a Liquid-Solid Interface Near the Angle of Incidence for Total Reflection," Applied Physics Letters, Vol. 7, No. 8 (1965).
9. C. E. Fitch and R. L. Richardson, "Ultrasonic Wave Models for Nondestructive Testing Interfaces with Attenuation," Progress in Applied Materials Research, edited by E. G. Stanford et. al., Iliffe Books, London, Vol. 8, 79-120 (1967).
10. F. L. Becker and R. L. Richardson, "Influence of Material Properties on Rayleigh Critical Angle Reflectivity," J. Acoust. Soc. Am., 51, 1609 (1972).
11. F. L. Becker, J. Appl. Phys., 42, 199-202 (1971).
12. C. E. Fitch, J. Acoust. Soc. Am., 40, 989-997 (1966).
13. F. L. Becker and R. L. Richardson, "Ultrasonic Critical Angle Reflectivity," Research Techniques in Nondestructive Testing, edited by R. S. Sharpe, Academic Press, London, 91-130 (1970).
14. F. L. Becker, C. E. Fitch and R. L. Richardson, "Ultrasonic Reflection and Transmission Factors for Materials with Attenuation," Battelle Memorial Inst. Report, BNWL-1283 (1970) (Unpublished).
15. V. M. Merkulova, Soviet Phys. Acoust., 15, 404 (1970).
16. F. L. Becker and R. L. Richardson, J. Acoust. Soc. Am., 51, 1609-1617 (1971).

17. B. G. Martin and F. L. Becker, "The Effect of Near-Surface Metallic Property Gradients in Ultrasonic Critical Angle Reflectivity," Materials Evaluation (1980).
18. F. L. Becker, "Ultrasonic Determination of Residual Stress," Battelle Pacific Northwest Laboratories (1973) (Unpublished Report).
19. B. G. Martin, Paper #6514, "Theory of the Effect of Stress on Ultrasonic Plane-Wave Reflectivity from a Water-Metal Interface," McDonnell Douglas Corp. (1978) (Unpublished Report).
20. B. P. Hildebrand and F. L. Becker, "Ultrasonic Holography at the Critical Angle," J. Acoust. Soc. Am., 56, 459-462 (1974).
21. H. L. Bertoni and T. Tamir, "Unified Theory of Rayleigh Angle Phenomena for Acoustic Beams at Liquid-Solid Interfaces," Appl. Phys. 2, 157-172 (1973).
22. H. L. Bertoni and Y. L. Hall, "Effects of Damping in a Solid on Acoustic Beams Reflected at the Rayleigh Critical Angle," in Proceedings of the 10th Symposium on Nondestructive Testing (NDE), 136, 142 (1975).
23. T. Tamir and H. L. Bertoni, "Lateral Displacement of Optical Beams at Multilayered and Periodic Structures," J. Opt. Soc. Am., Vol. 61, No. 10 (1971).
24. L. E. Pitts, "A Unified Theoretical Description of Ultrasonic Beam Reflections from a Solid Plate in a Liquid," Ph.D. Thesis, Georgetown University, Washington, D.C. (1976).
25. L. E. Pitts and T. J. Plona, "Theory of Nonspecular Reflection Effects for an Ultrasonic Beam Incident on a Solid Plate in a Liquid," IEEE Transactions on Sonics and Ultrasonics, Vol. SU-24, No. 2 (1977).
26. T. D. K. Ngoc and Walter G. Mayer, "Ultrasonic Nonspecular Reflectivity Near Longitudinal Critical Angle," J. Appl. Phys., 50(12) (1979).
27. T. D. K. Ngoc and W. G. Mayer, "Numerical Integration Method for Reflected Beam Profiles Near Rayleigh Critical Angle," J. Acoust. Soc. Am., Vol. 67, 1149-1152 (1980).
28. T. D. K. Ngoc, "Influence of Absorption in Ultrasonic Non-Specular Reflectivity," Ph.D. Thesis, Georgetown University, Washington, D.C. (1979).
29. K. W. Ng, "Nonspecular Ultrasonic Bounded Beam Transmission Through Solid Plates, Ph.D. Thesis, Georgetown University, Washington, D.C. (1979).

30. Robert Beyer, "New Wave of Acoustics," Physics Today (1980).
31. O. V. Rudenko and S. I. Soluyon, "Theoretical Foundations of Nonlinear Acoustics," in studies in Soviet Science series, Consultant Bureau, New York (1977).
32. R. Kompfner and R. A. Lemons, "Nonlinear Acoustic Microscopy," Appl. Phys. Lett., 28(b), 295-297 (1976).
33. R. E. Green, Ultrasonic Investigation of Mechanical Properties, Academic Press, New York (1973).
34. M. A. Breazeale, "Ultrasonic Studies of the Nonlinear Properties of Solids," International Journal of Nondestructive Testing, Vol. 4, Gorden and Breach, Great Britain (1972).
35. I. A. Viktorov, Rayleigh and Lamb Waves, Physical Theory and Applications, Plenum Press, New York (1967).
36. L. Knopoff and J. F. MacDonald, Rev. Mod. Phy., Vol. 30, No. 4, 1178-1192 (1958).
37. James A. Rooney and Wesley L. Nyborg, "Acoustic Radiation Pressure in a Traveling Plane Wave," Am. J. Phy., Vol. 40, 1825 (1972).
38. J. Zieniuk and R. C. Chivers, "Measurement of Ultrasonic Exposure with Radiation Force and Thermal Methods," Ultrasonics, 161 (1976).
39. Paul Lorrain and Dale R. Corson, Electromagnetic Fields and Waves, W. H. Freeman and Company, San Francisco, 546 (1962).
40. E. M. Lifshitz and L. P. Pitaevskii, Statistical Physics, 3rd edition, Part 1, Pergamon, Oxford (1980).
41. R. P. Feynman, Statistical Mechanics, W. A. Benjamin, Reading, MA (1972).
42. W. R. Beam, Electronics of Solids, McGraw-Hill, New York (1965).
43. R. Truell, C. Elbaum, and B. B. Chick, Ultrasonic Methods in Solid State Physics, Academic Press, New York (1969).
44. Carl M. Bender and Steven A. Orszag, Advanced Mathematical Methods for Scientists and Engineers, McGraw-Hill, New York (1978).

## 9.0 SUPPLEMENTARY REFERENCES

L. D. Landau and E. M. Lifshitz, Electrodynamics of Continuous Media, Pergamon Press, New York (1960).

E. P. Papadakis, "Revised Grain-Scattering Formulas and Tables," J. Acoust. Soc. Am., Vol. 37, No. 4 (1965).

A. L. Van Buren and M. A. Breazeale, "Reflection of Finite-Amplitude Ultrasonic Waves," J. Acoust. Soc. Am., Vol. 44, No. 4, 1014-1020 (1968).

O. I. Diachok and W. G. Mayer, "Crystal Surface Orientation by Ultrasonic Beam Displacement," Acustica, Vol. 26, 267-269 (1972).

Edmund G. Henneke II, "Reflection of an Elastic Wave at a Free Boundary in Hexagonal Metals," J. Acoust. Soc. Am., Vol. 53, No. 4, 1176 (1973).

Physical Acoustics, Vo. X, 61-126, edited by Warren P. Mason and R. N. Thurston, Academic Press, New York (1973).

M. A. Breazeale, Laszlo Adler, and Larry Flax, "Reflection of a Gaussian Ultrasonic Beam from a Liquid-Solid Interface," J. Acoust. Soc. Am., Vol. 56, No. 3 (1974).

L. D. Landau and E. M. Lifshitz, Theory of Elasticity, Pergamon Press, New York (1975).

Physical Acoustics, Vol. XII, 217-275, edited by Warren P. Mason and R. N. Thurston, Academic Press, New York (1976).

Edmund G. Henneke II and Gerald L. Jones, "Critical Angle for Reflection at a Liquid-Solid Interface in Single Crystals," J. Acoust. Soc. Am., Vol. 59, No. 1 (1976).

M. A. Breazeale and Michael A. Torbett, "Backward Displacement of Waves Reflected from an Interface Having Superimposed Periodicity," Applied Physics Letters, Vol. 29, No. 8, 15 (1976).

M. A. Breazeale, Laszlo Adler, and Gerald W. Scott, "Interaction of Ultrasonic Wave Incident at the Rayleigh Angle on a Liquid-Solid Interface," J. Appl. Phys., Vol. 48, No. 2 (1977).

Tran D. K. Ngoc and Walter G. Mayer, "A General Description of Ultrasonic Nonspecular Reflection and Transmission Effects for Layered Media," IEEE Transactions on Sonics and Ultrasonics, Vol. SU-27, No. 5 (1980).

A. H. Nayieh et. al., "Ultrasonic Leaky Waves in the Presence of a Thin Layer," J. Appl. Phys., 52(8) (1981).

K. W. Ng et. al., "Nonspecular Transmission Effects for Ultrasonic Beams Incident on a Solid Plate in a Liquid," Acustica, Vol. 48, No. 3 (1981).

Abdullah Atalar, "On the Reflection Coefficient Which Exceeds Unity," J. Acoust. Soc. Am., 70(4) (1981).

## APPENDIX A: FUNDAMENTAL BASIS FOR NONLINEAR NATURE OF ELASTIC WAVES

Sound is an inherently nonlinear phenomenon. Yet because of the possibility of expressing the motion of a solid body in "normal coordinates," it may be made to appear as an approximately linear phenomenon; thereby, obscuring its true nonlinear origins.

A solid body may be viewed in quantum mechanical terms as a collection of coupled harmonic oscillators.<sup>41</sup> Each oscillator corresponds to an atom or molecule of the solid. It is this coupling that allows a disturbance at one point in a medium to propagate to other points in the medium. This coupling is essential for without it no energy or momentum could be transferred, and no sound disturbance could propagate. Such interactions, of course, render the theory nonlinear at the outset.

A set of coupled quantum mechanical oscillators is described by the Hamiltonian<sup>41</sup>

$$H = \sum_i \frac{p_i'^2}{2M_i} + \sum_{ij} C_{ij}' q_i' q_j' \quad (1)$$

where  $q_i'$  are the coordinates of the amount of displacement from equilibrium of each oscillator and the momentum operator is

$$p_i' = \frac{\hbar}{i} \frac{\partial}{\partial q_i'} . \quad (2)$$

$C_{ij}'$  are nonzero coupling constants expressing the interactions among the oscillators. Making the change of variables,

$$Q_\alpha = \sum_i A_i^{(\alpha)} q_i = \sum_i A_i^{(\alpha)} \sqrt{M_i} q_i' \quad (3)$$

where  $A_i^{(\alpha)}$  are constants independent of time, one may "linearize" these equations in the first approximation. One finds  $H = \sum_\alpha H_\alpha$

where

$$H_\alpha = \frac{-\hbar^2 \partial^2}{2 \partial Q_\alpha^2} + 1/2 \omega_\alpha^2 Q_\alpha^2. \quad (4)$$

The eigenvalues of the "collective" Hamiltonian  $H$  may then be shown to be

$$E = \sum_\alpha (N_\alpha + 1/2) \hbar \omega_\alpha. \quad (5)$$

This equation gives the total energy of all "independent"  $\alpha$  sound modes present in the solid. A particular sound mode, say  $\alpha = 0$ , has energy

$$E = (N_0 + 1/2) \hbar \omega_0. \quad (6)$$

That is, the sound wave of frequency  $\omega_0$  consists of  $N_0$  phonons each with energy  $\epsilon_0 = \hbar \omega_0$  and momentum

$$\bar{P} = \hbar \bar{k} \quad (7)$$

$$|\bar{P}| = \frac{\epsilon_0}{v} \quad (8)$$

where  $v$  is the phase velocity of the sound wave. In the limit of large quantum numbers ( $N_0 \gg 1$ ), the energy of the sound wave goes over to the classical physics value, namely

$$E \approx N_0 \hbar \omega_0 = N_0 \epsilon_0 \quad (9)$$

and its corresponding momentum is

$$|\vec{P}| \approx \frac{E}{v} \quad (10)$$

which is the usual classical expression for momentum.<sup>37</sup>

Strictly speaking, if the coupling constants  $C_{ij}' = 0$ , there are no sound waves. Consequently, they carry neither energy or momentum. We see from this exercise that although a fundamentally nonlinear phenomenon (sound) may look linear in the classical approximation (in the normal coordinates), it is not. Thus, we must use care, in classical phenomenological treatments of a sound wave, not to eliminate important physical effects by using only linear equations which are fundamentally incorrect. The existence of interactions between atoms in a solid, of course, always leads to inevitable losses.

It is also evident from the foregoing discussion that there is, strictly speaking, no lossless case in acoustics. One must, therefore, be careful in treating real problems by first examining lossless, linear cases and then making small phenomenological

corrections to account for losses and nonlinearities. Such an approach could, in some cases, fail to incorporate important physical effects and, at the very least, tends to obscure physical relationships.

